EUROPEAN SOUTHERN OBSERVATORY

Organisation Européene pour des Recherches Astronomiques dans l'Hémisphère Austral
Europäische Organisation für astronomische Forschung in der südlichen Hemisphäre

ESO - European Southern Observatory
Karl-Schwarzschild Str. 2, D-85748 Garching bei München

Very Large Telescope
Paranal Science Operations
ESPRESSO User Manual

Issue 111.1, Date 22/03/2023

M. Jones and E. Sedaghati
(original by P. Molaro, P. Figueira, A. Mehner, G. Lo Curto and the ESPRESSO consortium)

Prepared . . . . . .

S. Mieske

Approved . . . . . .
Date Signature

A. Kaufer

Released . . . . . .
Date Signature

This page was intentionally left (almost) blank.

Change Record

Issue/ Rev.	Date	Section/Parag. affected	Reason/Initiation/Documents/Remarks
v0.1	2017/02/01	all	First draft
v0.5	2017/02/28	all	PAE version
v0.6	2018/02/06	all	F. Pepeś revision
v0.8	2018/03/01	all	Version for ESO Period 102
v1.0	2018/07/01	all	Version for Phase 2 submission
v1.1	2018/09/01	all	Updated version for Period 103
v1.2	2018/12/18	all	Updated version for Period 103, phase 2
v1.3	2019/03/04	all	Updated version for Period 104
v1.4	2019/08/25	all	Updated version for Period 105
v2.0	2019/11/21	all	Major update of the manual
v2.1	2020/02/23	6.1.2, 6.2.4, 6.2.6, 6.4	New sections on RV precision by the ETC, time series preparation, blind offsets, and observing with 4UT.
v2.2	2020/05/22	6.1.2, 6.2.1, 6.3.1	Improved description on RV precision by the ETC and on the measurement of IQ during acquisition.
v2.3	2020/07/08	3.3.3, 6.2.5, 8.3	correction of typos, mention of VLT's airmass limit, pipeline results across architectures
v2.4	2020/09/23	6.2.5	instructions for time-critical OBs, typos correction
v2.5	2020/10/05	1.2, 8.0	new reference for ESPRESSO paper
v2.6	2020/11/30	4.4, 5.3, 6.2.1, 6.2.4	description of SINGLEHR42, of CT-induced interference, and of blind offset acquisition magnitude
v2.7	2021/05/24	6.2.1	information on SpTp usage
v2.8	2021/06/11	5.4, 5.5	new sections on known issues
v2.9	2021/08/30	6.2.7	new section on common OB preparation
v2.10	2021/09/28	6.4	mistakes "Guide Star preparation tool" replaced by "p2/ObsPrep tool"
v2.11	2023/03/22	2.3, 3.4, 5.3, 5.4, 6, 7, 8	Definition of an accurate Wavelength Calibration, The Calibration Unit, Blue Cryostat Temperature instabilities, Observing with ESPRESSO, Calibration plan, Interference pattern and new section Detector's cryostats intervention.
v2.12	2023/11/19	5.6, 6.2, 7.2.1, 7.2.4	EM de-synchronization, Instrumental stability, Template parameters, Using blind offsets.
v2.13	2025/05/24	2, 7.2.6, 8	ESPRESSO Science Drivers and Scientific background, Time series (updated TSP link), Calibration Plan
v2.14	2026/04/24	3.4.1	New sub-section on the LFC

Contents

1 Introduction **1**
1.1 Scope of this document . . . 1
1.2 Additional information on ESPRESSO . . . 1
1.3 Structure of this Manual . . . 2

2 ESPRESSO Science Drivers and Scientific background **3**
2.1 Calculating Precise RVs . . . 3
2.2 Illumination Stability and Mechanical Stability . . . 5
2.3 Definition of an accurate Wavelength Calibration . . . 6
2.4 The importance of slit losses . . . 6

3 Instrument description **8**
3.1 The Coudé Train . . . 8
3.2 The Front End . . . 9
3.3 The Spectrograph . . . 11
3.3.1 Optical Design . . . 11
3.3.2 Opto-mechanics and Themal Control . . . 13
3.3.3 The Scientific Detectors . . . 13
3.4 The Calibration Unit . . . 15
3.4.1 The Laser Frequency Comb . . . 16

4 Configuring ESPRESSO **19**
4.1 Instrument Modes . . . 19
4.2 Source on the reference Fibre . . . 20
4.3 Detector Readout Modes . . . 21
4.4 Instrument configurations . . . 21

5 Instrument performance and known issues. **23**
5.1 Total Efficiency and on-sky RV precision . . . 23
5.2 Dark Current, Diffused Light, Ghosts, and Sky Background . . . 25
5.3 Interference pattern introduced by the Coudé Train . . . 25
5.4 Blue Cryostat Temperature instabilities (before May 2022) . . . 26
5.5 ADC/PLC issues on Jan-Apr 2021 . . . 27
5.6 Exposure meter de-synchronization (Oct. 2021 to Aug. 2023) . . . 28

6 Detector's cryostasts repair intervention **29**
6.1 Spectral format . . . 29
6.2 Instrumental stability . . . 30
6.3 Replacement of the NGCs front end boards . . . 32

7 Observing with ESPRESSO **32**
7.1 Using the ETC to prepare observations . . . 33
7.1.1 Turbulence Categories and Constraints . . . 33
7.1.2 RV precision from the ETC . . . 34
7.2 Preparation of P1 and P2 material . . . 34
7.2.1 Template parameters . . . 35
7.2.2 Finding Charts . . . 36
7.2.3 Limiting magnitude for acquisition . . . 36
7.2.4 Using Blind Offsets . . . 36
7.2.5 OB constraints . . . 36
7.2.6 Time series . . . 38
7.2.7 Common mistakes to avoid when preparing the observations . . . 39
7.3 A summary of observations . . . 39
7.3.1 The Acquisition . . . 39
7.3.2 The Exposure Meter . . . 40
7.3.3 The Integration . . . 41
7.3.4 Quality Control – QC0 . . . 41
7.4 Preparing observations and Observing with 4UT . . . 41

8 Calibration Plan **43**

9 Software for an End-to-End Operation **45**
9.1 Data Reduction Software (DRS) . . . 45
9.2 Data Analysis Software (DAS) . . . 45
9.3 Pipeline results across architectures . . . 46

Appendix A ESPRESSO Spectral Format **47**

List of acronyms

1T	First temperature enclosure (convergence-point room)
3T	Third temperature enclosure (surrounding the vacuum vessel)
ADC	Atmospheric Dispersion Corrector
APSU	Anamorphic Pupil Slicer Unit
BOB	Broker of Observation Blocks
CCD	Charge-Coupled Device
CCL	Combined Coudé Laboratory
CPL	Common Pipeline Library
CR	Coudé Room
CTE	Charge Transfer Efficiency
DAS	Data Analysis Software
DFS	Data Flow System
DRS	Data Reduction Software
EG	Echelle Grating
EM	Exposure meter
ESPRESSO	Echelle Spectrograph for Rocky Exoplanets and Stable Spectroscopic Observations
ETC	Exposure Time Calculator
FE(U)	Front-End (Unit)
FP(CS)	Fabry-Pérot (Calibration Source)
FWHM	Full-Width at Half-Maximum
GUI	Graphical User Interface
HARPS	High-Accuracy Radial-velocity Planet Searcher
HDU	Header/Data Unit
HR	High Resolution
ICCF	Incoherent Conbined Coudé Focus
IOT	Instrument Operations Team
LDLS	Laser-Driven Light Source
LFC	Laser Frequency Comb
OB	Observation Block
PAE	Provisional Acceptance Europe
PCF	Photonic Crystal Fibre
PLC	Programmable Logic Controller
RV	Radial Velocity
RON	Read-Out Noise
S/N	Signal-to-Noise Ratio
SU	Scrambling Unit
SW	Software
TCCD	Technical CCD
UHR	Ultra-High Resolution
UT	Unit Telescope (8.2-metre telescope at Paranal)
VLT	Very Large Telescope
VPHG	Volume Phase Holographic Grating
VV	Vacuum Vessel

1 Introduction

1.1 Scope of this document

The ESPRESSO User Manual was written to assist science users during phase 1 (Call for Proposals) and phase 2 (observations preparation) by providing the necessary information on the instrument capabilities and its operation. This document provides:

- A brief description of ESPRESSO Science Drivers;
- An overall description of ESPRESSO technical characteristics, its observing modes, and performances;
- Practical Information on the preparation and execution of observations;
- The calibration plan of the instrument;
- A brief introduction to the pipeline data reduction and data analysis software.

The different versions of this manual, along with the companion *ESPRESSO Template Manual* can be found at:

https://www.eso.org/sci/facilities/paranal/instruments/espresso/doc.html

The content presented here is based on material provided by the ESPRESSO Consortium. Comments and suggestions are welcome and should be addressed to the User Support Department (*usd-help@eso.org*).

1.2 Additional information on ESPRESSO

The complete ESPRESSO documentation is available from the ESPRESSO public web pages, along with the latest news on the instrument:

http://www.eso.org/sci/facilities/paranal/instruments/espresso

Information and software tools for the preparation of service- and visitor-mode observations using ESPRESSO are available at:

https://www.eso.org/sci/observing/phase2/SMGuidelines/Documentation.ESPRESSO.html

Visiting astronomers will find instructions on the Paranal Science Operations web pages as well as the dedicated ESPRESSO page:

http://www.eso.org/sci/facilities/paranal/sciops
http://www.eso.org/sci/facilities/paranal/instruments/espresso/visitor

For a daily update on the Health Check of the instrument please take a look at:

http://www.eso.org/observing/dfo/quality/HEALTH/KPI/InstrPerf_ESPRESSO.html

Publications using ESPRESSO observations should cite the paper:

Pepe et al. (2020) "ESPRESSO@VLT – On-sky performance and first results"

1.3 Structure of this Manual

The ESPRESSO User Manual is structured as follows. In Section 2 we present the ESPRESSO science drivers and the key concepts behind the instruments' design. A brief description of ESPRESSO's inner workings is provided in Section 3, and the possible instrument configurations are presented in Section 4. In Section 5 we describe the instrument's performance, while in Section 6 the main results and improvements after the instrument intervention in 2022. In Section 7 the main aspects to keep in mind when preparing observations and observing with ESPRESSO are presented. The calibration plan is detailed in Section 8 and the software suite supporting ESPRESSO presented in Section 9. Finally, a description of the ESPRESSO Spectral Format is provided in Appendix A.

2 ESPRESSO Science Drivers and Scientific background

The ESPRESSO spectrograph was designed to meet two scientific objectives:

- the detection of an Earth-Mass exoplanet orbiting inside the habitable zone of a Sun-like star;
- the measurement of the potential variation of the fundamental constants of the Universe.

The first goal imposes on ESPRESSO a Radial Velocity (RV) precision (or stability) of $\sim$ 10 cm/s. This value corresponds to the RV semi-amplitude of an Earth-Mass planet orbiting inside the habitable zone of a G-type star. Since this measurement requires the acquisition of data over several years, this precision level should be maintained over a timescale of up to ten years. This precision can only be reached by averaging thousand of spectral lines, allowing us to measure a relative shift between two spectra at this level. Hence this is not the precision on a single line (which is at the several m/s level, depending on the S/N).

The precision of a measurement system, also called reproducibility or repeatability, is the degree to which repeated measurements under unchanged conditions lead to the same results. On the other hand, the accuracy of a measurement system is the degree of closeness between its measurements of a quantity and the quantity's real value. The measurement of fundamental constants imposes a very accurate (absolute) local wavelength calibration of $\sim$ 5-10 m/s on single lines. When operating at this accuracy level, the observation of the Lyman-alpha forest created by the interstellar medium absorption on distant quasars light allows one to measure the potential variation of fundamental constants through space and time.

The two goals can be achieved by an extremely stable high-resolution spectrograph capable of resolving the stellar and quasar lines. The RV precision required imposes strong constraints on the stability of the spectrograph, while the needed accuracy has an additional impact on defining an accurate wavelength calibration system.

2.1 Calculating Precise RVs

In a first approximation, the precision of an RV measurement σ_{RV} measured on a high signal-to-noise (S/N) spectrum of unresolved stellar lines depends on (e.g., Cochran & Hatzes 1990)

$$\sigma_{RV}^{-1} \propto \sqrt{F}\,\sqrt{\Delta\lambda}\,R^{1.5} \tag{1}$$

in which F is the average continuum flux measured on the spectrum, $\delta\lambda$ the spectral wavelength coverage and R the resolution at which it is observed.

The term $\sqrt{F}$ represents the S/N contribution, and shows that the RV precision measured on a single line is inversely proportional to the S/N. This term shows the importance of maximizing the transmission of the spectrograph's optical components and reducing their number so that the overall instrument transmission is as high as possible.

When averaging the RV measured over N different lines, and if one considers these as independent measurements, the stacking leads to a gain $\propto \sqrt{N}$. If one assumes that spectral lines

are distributed homogeneously over the available wavelength range, the gain in precision by increasing (or reducing) the wavelength coverage is given by the term $\sqrt{\Delta\lambda}$.

The term $R^{1.5}$ represents the gain in spectral information obtained by increasing the resolution of the spectrograph. If one increases the resolution, the spectral lines becomes both deeper and narrower. Since the RV precision measured on a line is proportional to its depth and inversely proportional to $\sqrt{FWHM}$, two quantities controled by resolution, this leads to the steep dependence and the factor of 1.5 (see e.g. Connes 1996; Bouchy, Pepe & Queloz 2001; Pepe et al. 2002).

The working assumption is that we are observing non-resolved spectral lines, i.e., lines for which the FWHM *before the light is dispersed by the spectrograph* is smaller than the broadening induced by the spectrograph's measurement, often known as $FWHM_{inst}$. The slowest-rotating G, K, and M stars have $v \sin i$ ~2.0 km/s, which translates to a limit resolution of $R \sim 150\,000$; above this value the gain is less steep and the coefficient 1.5 is not representative.

Equation 1 allows us to estimate the spectral information content of a spectrum after being dispersed, but does not consider the effects of digitation, i.e., how the spectrum is recorded on the detector. This aspect is characterized by the sampling: the number of pixels used to record $FWHM_{inst}$[1]. From the Nyquist-Shannon Sampling Theorem we get that two or more points per cycle of highest frequency allow the reconstruction of band-limited functions, i.e., at least 2 points per $FWHM_{inst}$ are necessary to reconstruct the signals we are trying to sample. Conversely, to reconstruct the frequencies required to measure the geometric center of a line with the highest fidelity, more than two pixels should be used. However, when adding extra pixels we are distributing the photons over a larger number of measuring devices that have a measurement error on their own. Even for the case of an infinite S/N the information gain on adding extra pixels becomes negligible.

In ESPRESSO a sampling larger than 2 was targeted in order to allow for a more precise and accurate measurements of the line centers. However, the optimal number of pixel depends on the spectra S/N, which brings us to the next concept: binning.

Binning defines how many pixels in X and Y dimension are read out simultaneously. For ESPRESSO, in an NxM binning, N pixel are clocked (transferred) in the spatial or cross-dispersed direction and M pixel in the dispersion direction, being read all at once. In this way the readout-noise contribution is accounted for only once, in opposition to contributing NxM times in the absence of binning. The binning scheme is thus favorable for low S/N observations that are read-out-limited (or close to this regime). The price to pay is a reduced sampling of the spatial profile (by a factor of N) and a reduced sampling of the lines in the dispersion direction (by a factor of M).

This brief section shows us why ESPRESSO was designed as a spectrograph with a high transmission, capable of collecting spectra over a wide wavelength range, and at a very high resolution. It also shows us the interest of using a high sampling, and that by binning we can adapt the sampling as a function of S/N. We are naively assuming that our spectrograph is a perfect measuring system. Close, but not really so.

[1] Also called numerical resolution, the sampling should not be confused with the resolution R.

2.2 Illumination Stability and Mechanical Stability

A spectrograph will disperse and re-image the light it receives at its interface focal plane (usually a slit or a fiber). A change in the distribution of light intensity on the focal plane (often called the *near-field*) or the geometrical direction of the incoming rays that form the image (often called the *far-field*) will propagate throughout the spectrograph and change the physical position of the spectral lines on the detector. For this reason, the light received by the spectrograph should be as stable as possible as a function of time . This means that the light feeding system should be as insensitive as possible to atmospheric effects (like seeing variations, and atmospheric turbulence in general) and to centering effects (that lead to only a fraction of the light of the stellar disk entering the spectrograph).

By using a fiber to scramble the light one ensures an homogeneous light distribution at the end of the fiber and into the spectrograph, rendering the spectra virtually insensible to light distribution variations. Moreover, the use of a double-scrambling optical system ensures scrambling of both the near-field and the far-field of the light beam. Modern fibres are manufactured with a polygonal cross-section; the non-circular cross section breaks the radial symmetry of the waveguide, and with it the geometric regularity the internal reflections inside the fibre, attaining a more homogeneous light distribution at the exit. Recent works show that the best scrambling is achieved using octagonal fibres (e.g., Chazelas et al, 2012, SPIE, V. 8450, p9). Since a variation of the light distribution at the entrance of the spectrograph can be translated into a position of the lines on the detector, a high scrambling and illumination is necessary for line position stability and the measurement of precise RVs.

Given that the light traverses the spectrograph and interacts with the different optical components inside it, the location of the lines on the detector will depend on the position of each optical element. To obtain the most repeatable line center measurement possible, the optical setup of the spectrograph should thus be kept fixed. For the same reason the refractivity index of the air should be kept as small and constant as possible. Following this reasoning, the high-precision RV spectrographs are stabilized in pressure P and temperature T, the two parameters running the refraction index $n \equiv n(P,T)$.

Even when going to such length to minimize instrumental RVs, residual effects will remain that are very difficult to prevent by design. Among these are, for instance, the warm-up of the detector as the electronics read-out. The reading process increases the temperature of the detector, which will in turn change its dimensions by dilation or thermal expansion. As this happens, the position on the detector where the lines are imaged will shift with the cooling cycle stage. This detector "breathing" and other residual effects can only be measured by using a simultaneous reference: a calibration source that goes through the spectrograph over the same optical path as that of the science target. In order to avoid the overlapping of spectra and blending of spectral features coming from the two sources, a parallel fiber is used. This fiber sends light over a geometrical path very close to that of the science target, to the point that the optical paths can be assumed to be the same. As such, any instrumental RV variation affecting the scientific target will be measured on real time on the reference fiber and can be subtracted directly. This simultaneous residual measurement is called "drift" and can be used to monitor the spectrograph's parasite instrumental RVs. For many years this simultaneous calibration was performed using Thorium-Argon (ThAr) lamps but today we employ Fabry-Pérot (FP) etalons that provide a higher density of sharp, stable and uniformly distributed lines.

These concepts have been applied and perfected by the team of Michel Mayor, from the seminal optical design of ELODIE (Baranne et al. 1996) and CORALIE, to HARPS and HARPS-N, and finally into ESPRESSO. They are the result of several decades of experimentation motivated by the strong scientific drive of exoplanet detection.

2.3 Definition of an accurate Wavelength Calibration

Illumination and mechanical stability, along with a simultaneous reference, allow us to create a precise measurement system but do not ensure accuracy, i.e., they do not ensure that wavelength or RV measurements are close to reality. That concerns wavelength calibration accuracy.

The wavelength calibration assigns to each detector pixel a wavelength value. In ESPRESSO this must be done with an error of $\delta\lambda/\lambda = 10^{-8}$. Unfortunately, none of the traditionally used calibration sources, such as ThAr lamps or Iodine cells, provide a spectrum with a high enough density of uniform and stable spectral features, spanning the whole wavelength range of ESPRESSO and with wavelengths values that can be referenced back to fundamental physics.

ESPRESSO can be wavelength-calibrated using either the ThAr lamp plus the FP spectra or the Laser Frequency Comb (LFC). The LFC provides a link to the frequency standard, allowing the higher wavelength accuracy of the two methods.

Currently, a combination of Th-Ar frames and FP exposures define the wavelength-calibration solution across the two detectors. The absolute reference wavelength defined by the Thorium lines are extended by the equidistant grid supplied by the FP, allowing us to extend the absolute reference in a more homogeneous and precise way than can be done with the Thorium lines alone.

As stated before, the same FP is used for simultaneous drift measurement. Note, however, that this reference source was designed for precision and not for accuracy. The LFC is not used at night for drift measurement due to its limited wavelength range (little flux bluer than $\sim 420\,\mathrm{nm}$) and reduced lifetime.

2.4 The importance of slit losses

A significant fraction of the incoming light is lost at the light-feed interface of the spectrograph; these are called *slit losses*. The slit losses for on a fiber-fed spectrograph are well approximated by

$$slit\,losses = exp(-0.53 \times (d/IQ)^2) \tag{2}$$

where d is the fiber diameter (on ESPRESSO $1''$ for singleHR and multiMR modes, and $0.5''$ for singleUHR mode) and IQ the image quality. IQ represents the image quality unaffected by the instrument transfer function, as seen at the focal plane of the slit or fiber. The IQ should not be mistaken for the seeing: while seeing is a measurement of the turbulence on the sky as seen on zenith, IQ is a measurement of the image size created by that turbulence measured through a specific optical system. For the mathematical relation between the two, please refer to the ETC help pages.

The IQ is well approximated by the image of the TCCDs on the slit/fiber viewer, as long as the image is not affected by pixelization issues and has a similar central wavelength to that of the instrument.

From Eq. 2 we conclude that slit losses become significant when $IQ \geq d$. This is an important aspect to consider when preparing observations. When in doubt, please refer to the ESPRESSO ETC for an estimation of the S/N achievable on your target with a given setup and conditions, and use this information when preparing your observations.

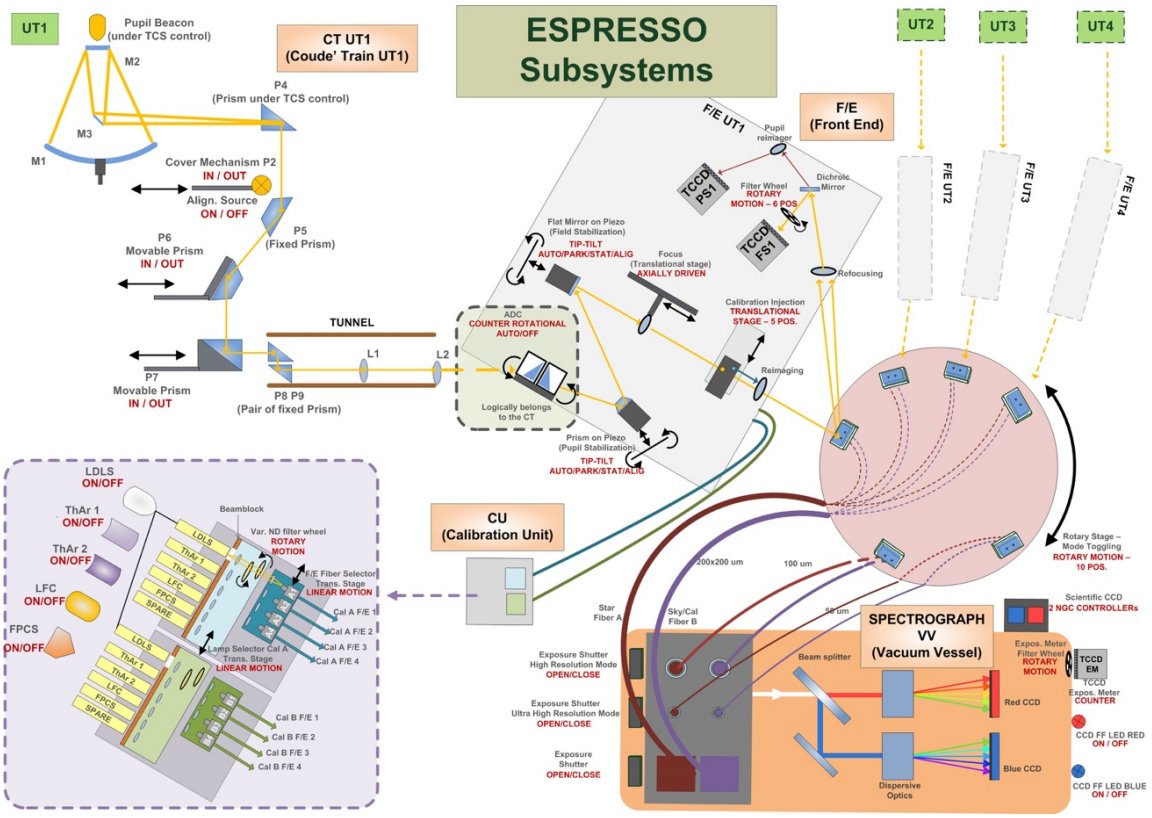

Figure 1: ESPRESSO and its different subsystems: Coude Train, Front-End, Calibration Unit and Spectrograph.

3 Instrument description

ESPRESSO is a fibre-fed, cross-dispersed, high-resolution Echellé spectrograph. The instrument is located in the Combined-Coudé Laboratory (CCL), and can collect light from the incoherent focus front-end units of the Unit Telescopes (UTs). The telescope light is fed from each of the UTs into the CCL via a Coudé-Train optical system, and then into the instrument through optical fibres. Target and reference light enter the instrument simultaneously through two separate fibres.

ESPRESSO is composed of four different subsystems: the Coudé Train, the Front Ends, the Calibration Unit, and the spectrograph. These are represented in Fig. 1 and described in the following sections.

3.1 The Coudé Train

The Incoherent Combined-Coudé Focus (ICCF) is the convergence point for the light of the four VLT UTs and is located in the CCL. Although foreseen in the original VLT plan, the ICCF was put to use for the first time with ESPRESSO. Using it, the instrument can receive light from any number or combination of the four UTs. The standard operation modes are 1-UT mode and 4-UT mode, in which light is fed from one or the 4 UTs, respectively.

The redirection of light from the telescopes to the CCL is obtained through a full optics solution, without using fibres. The Coudé Trains pick up the light at the level of the Nasmyth-B platforms and redirect it using 4 prisms through the UT mechanical structure, down to the

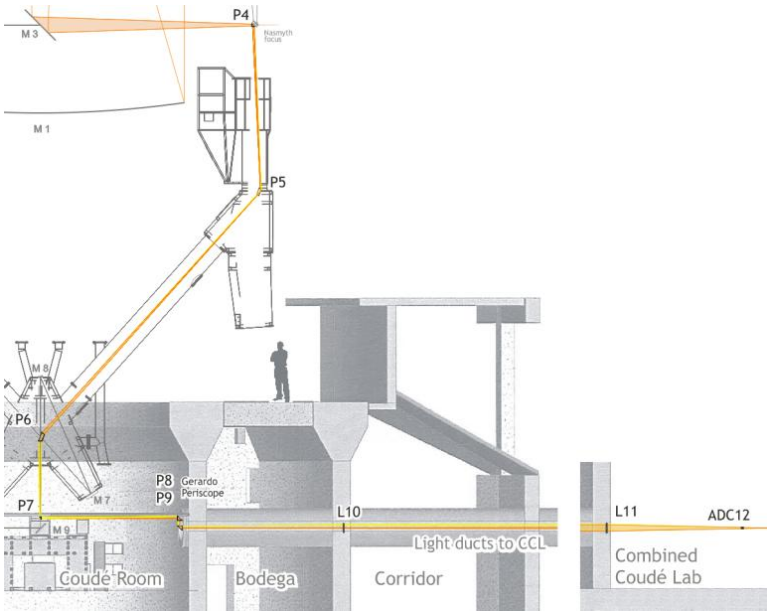

Figure 2: UT Coudé Train and optical path to the CCL through the telescope and tunnels.

UT Coudé Rooms (CR). It is then directed along the incoherent light ducts into the CCL (see Fig. 2) by using a 2-mirrors periscope and 2 lenses. In this way, the beams from the four UTs converge into the CCL, and to a Front-End (FE) sub-system for each of the UTs. The implementation of the Coudé Trains required substantial changes in the Paranal Observatory infrastructure resulting in a sophisticated interface management.

3.2 The Front End

The Front-End (FE) sub-system is composed of a rigid four-arm structure, with each arm oriented towards one of the UT's incoherent tunnels, and four FE units. The beam received from the Coudé is corrected for atmospheric dispersion by a dedicated Atmospheric Dispersion Corrector (ADC) unit (one per FE) and then redirected to the common focal plane where the heads of the fibre-to-spectrograph feeding are located. While performing beam conditioning, the FE can apply pupil and field stabilization via two independent control loops, each composed of a technical CCD and a tip-tilt stage. Due to ESPRESSO having a very stable pupil, the pupil stabilization control loop is currently not in use.

In addition to these functions, the FE allows the injection of calibration light into the spectrograph. An inside view of a single FE Unit and its main components is provided in Fig. 3. In this figure, the beam arrives through the tunnel and crosses the ADC (on the right-hand side, outside of the figure). After that is deflected by the pupil- and field-stabilisation mirrors towards the fibre head, where the light is injected into the fibre link through a pinhole in the field mirror. A refocusing mechanism allows to focus the stellar image on the pinhole for optimum efficiency. The field mirror redirects the beam falling outside of the pinhole towards a guiding field and a pupil cameras for field and pupil visualizations, respectively, which provide a positive feedback to the pupil- and field-stabilisation mirrors. A top view of the whole FE sub-system is shown in Fig. 4, together with a picture of the interior of the CCL.

The Fibre-Link sub-system relays the light from the FEs to the spectrograph. The 1-UT mode uses 2 octagonal fibres, one for the object and one for either the sky or for simultaneous radial-velocity reference.

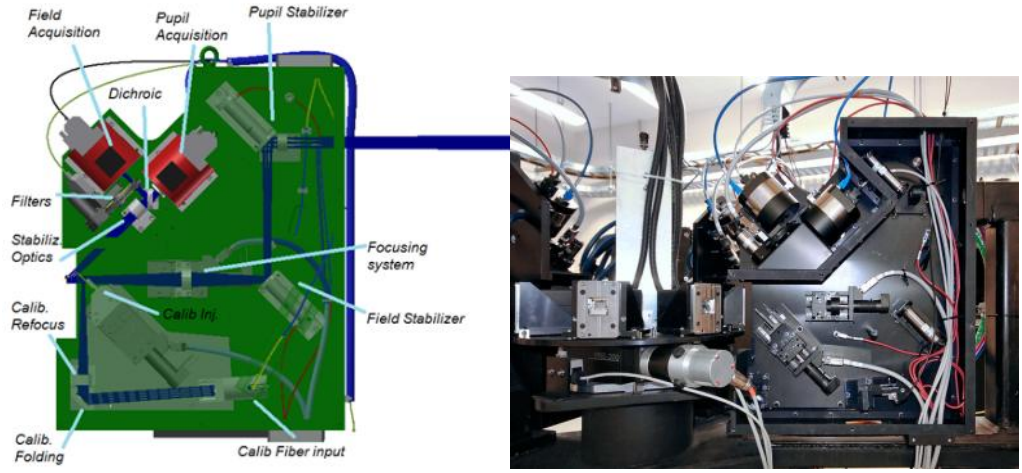

Figure 3: Side View of an individual front-End Unit.

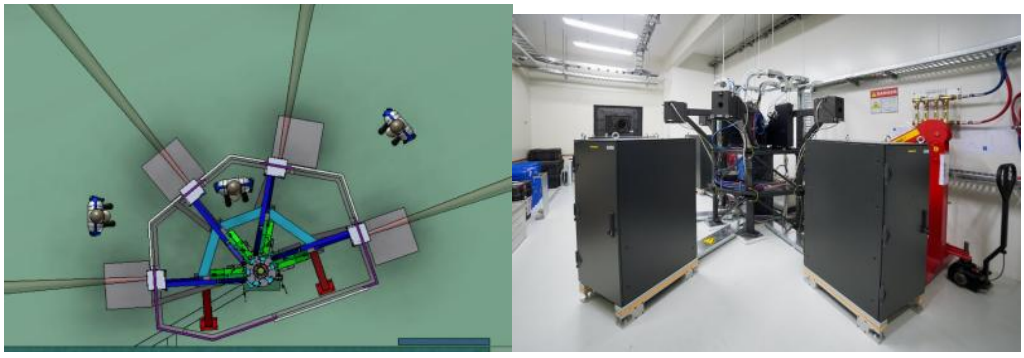

Figure 4: Schematic top view of the Front-End Sub-System (*left*) and view FE and the four UT beams in the CCL (*right*).

In the 1-UT high-resolution mode (named singleHR), the fibres have a core of 140 μm that subtends 1″on the sky. In the ultra-high resolution (singleUHR) mode, the fibres' core is 70 μm wide, equivalent to 0.5″on the sky. The two fibre pairs are located in separate bundles mounted on a rotary device that permits the alignment with the focal plane of the FE of the corresponding UT. In the 4-UT mode (multiMR), four object fibres and four sky/reference fibres converge from the four UTs. The four object fibres, all with a core of 140 μm wide, are bundled together to feed a single square 280 μm wide object fibre; the same procedure is used for the four sky/reference fibres that feed a single square 280 μm wide sky/reference fibre. Thus, in the 4-UT mode, the spectrograph creates a dispersed image of a fibre twice as wide as in the case of the 1-UT fibres.

While feeding of the light from the FEs into the spectrograph, the Fibre-Link performs the essential task of light scrambling. By doing so, it minimizes the negative effects of atmospheric turbulence and poor target centering, as discussed on Section 2.2.

3.3 The Spectrograph

The spectrograph is (only) one of the components of the ESPRESSO instrument. To design it, several innovative optical solutions were used to obtain simultaneously high spectral resolution, high efficiency, and high mechanical stability.

3.3.1 Optical Design

The optical design of the spectrograph is shown in Fig. 5. To minimize the dimension of the optics, particularly those of the collimator and of the Echelle grating, ESPRESSO implements anamorphic optics. At the spectrograph's entrance, the Anamorphic Pupil Slicing Unit (APSU) compresses the beam in cross-dispersion direction and a pupil slicer splits the pupil into two beams; the two are superimposed on the Echelle grating, that through this optical trick can have a smaller size. The rectangular white pupil is then re-imaged and compressed. After the main dispersion, the dichroic beam splitter separates the beam into blue and red spectroscopic arms; the independent arms can then be optimized for image quality and optical efficiency. The cross-dispersers, that come after this step, separate the overlapping pre-dispersed spectral orders. After it, an anamorphism is re-introduced to re-shape the pupil into a square and to compress the order height such that the inter-order spacing and the signal-to-noise ratio (S/N) per pixel are maximized. Both functions are accomplished using Volume Phase Holographic Gratings (VPHGs) mounted on prisms. The shape and size of both the pupil and fibre images are shown in Fig. 6 for various locations along the optical beam of the spectrograph. Finally, two optimised camera lens systems image the full spectrum from 380 nm to 788 nm on two large 92 mm x 92 mm CCDs with 10 μm pixels.

Without the application of the anamorphic pupil design, the collimator beam size would have a diameter of 40 cm and the Echellé grating would have a size of 180 cm x 40 cm. Instead, ESPRESSO employs an Echellé grating of 120 cm x 20 cm and much smaller optical elements (collimators, cross dispersers, etc.). Due to the elongated shapes of the image of the two slices, each spectral element is covered by a larger number of detector pixels. To avoid increased detector noise on low S/N observations, pixel binning is available. On the other hand, by spreading the flux across a larger number of pixels one can reach a higher S/N per single exposure, a significant advantage in the high S/N regime. The resulting (general) spectral

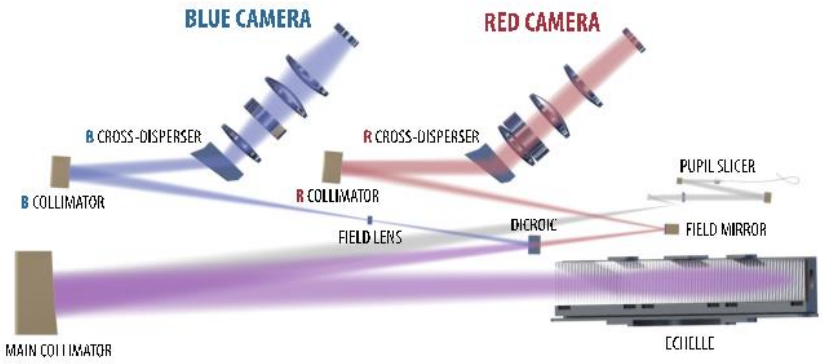

Figure 5: Schematic layout of the ESPRESSO spectrograph and its optical elements.

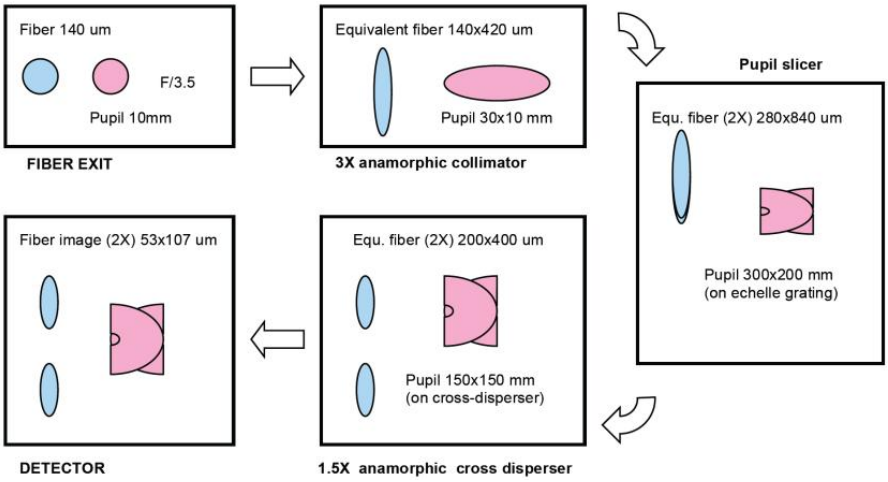

Figure 6: Conceptual description of pupil and fibre images at key locations inside the spectrograph.

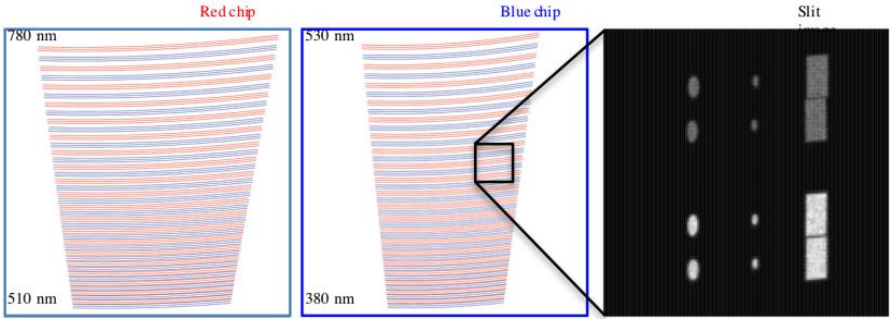

Figure 7: Format of the spectrum on the red and blue scientific detectors. On the right we have a zoom-in on the pseudo-slit image, with the image of the target (*bottom*) and sky fibre (*top*). Each fibre is re-imaged into two slices, aligned vertically. The image of the pseudo-slit on the science detectors, from left to right: in the 1-UT UT mode, in the 1-UT UHR mode, and in the 4-UT MR mode.

format covered by the blue and red chips as well as the images of the pseudo-slits on the science detectors are shown in Fig. 7.

3.3.2 Opto-mechanics and Themal Control

ESPRESSO was designed to be an ultra-stable spectrograph capable of reaching an RV precision of the order of 10 cm/s, i.e., one order of magnitude better than the goal RV stability of its predecessor, HARPS. To this aim, the spectrograph has a fully fixed configuration for the highest thermo-mechanical stability. The optics are mounted on a tri-dimensional optical bench specifically designed to keep the optical system within the thermo-mechanical tolerances required for high-precision RV measurements. The bench is located inside a vacuum vessel where a 10^{-5} mbar class vacuum is permanently maintained. An overview of the opto-mechanics of the spectrograph is shown in Fig. 8. The temperature of the optical system is stabilized at the mK level to avoid optical index refraction variations and triggering mechanical instabilities. This requirement is fulfilled by locating the spectrograph in an active multi-shell thermal enclosure system, depicted in Fig. 9 and Fig. 10. Each shell improves the temperature stability by a factor of 10, thus getting from typically Kelvin-level variations in the CCL down to mK stability inside the vacuum vessel and on the optical bench.

3.3.3 The Scientific Detectors

ESPRESSO implements several innovative solutions for scientific CCDs, their packages, and cryostats. One of the world's largest monolithic CCDs was selected to cover the spectral format and wavelength range of ESPRESSO and to obtain improved stability when compared to a mosaic solution like that employed in HARPS. The CCDs were procured from the *e2v* supplier and have a sensitive area of 92 mm x 92 mm, composed of 9k9 pixels of 10 μm size. Fast read-out of such a large chip is achieved by using 16 output ports at high speed. The scientific CCDs have very demanding specifications in terms of parameters like Charge Transfer Efficiency (CTE) and pixel position homogeneity, on which an error translates directly into the RV precision and accuracy. An engineering sample is shown in Fig. 11. For better stability and thermal-expansion matching, the CCD package is made of Silicon Carbide. ESPRESSO's target precision of 10 cm/s requires measuring spectral line position changes of 2 nm in the CCD plane, equivalent to only 4 times the silicon lattice constant. The CCDs package, the

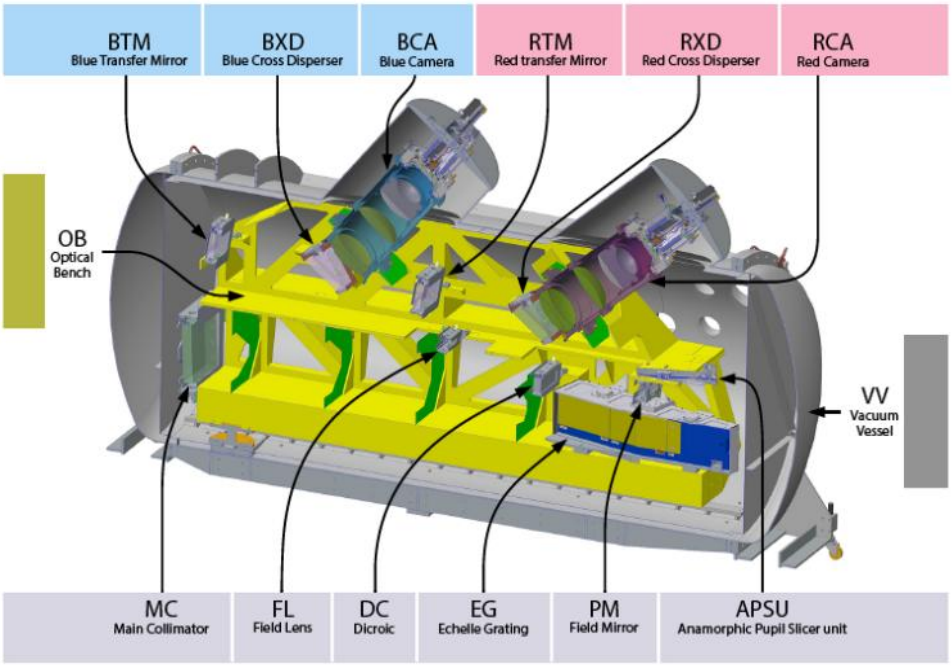

Figure 8: Opto-mechanics of the ESPRESSO spectrograph.

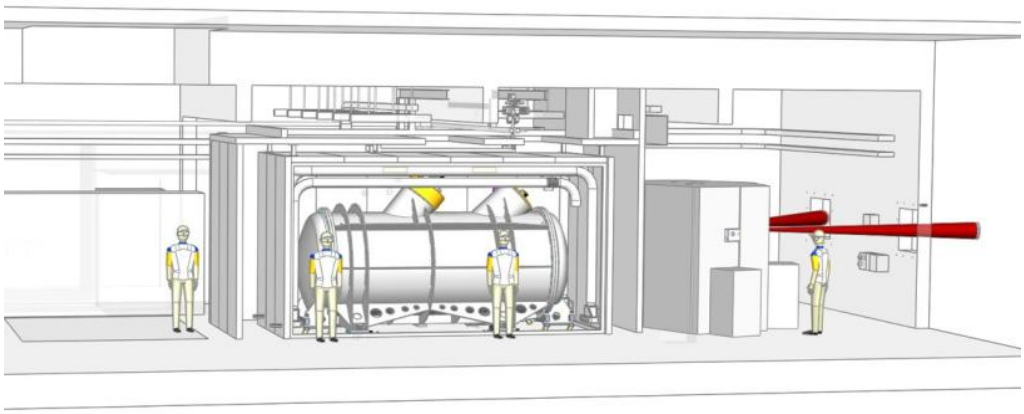

Figure 9: Representation of ESPRESSO inside the CCL, vacuum vessel and multi-shell thermal control system, with converging light beams represented in red.

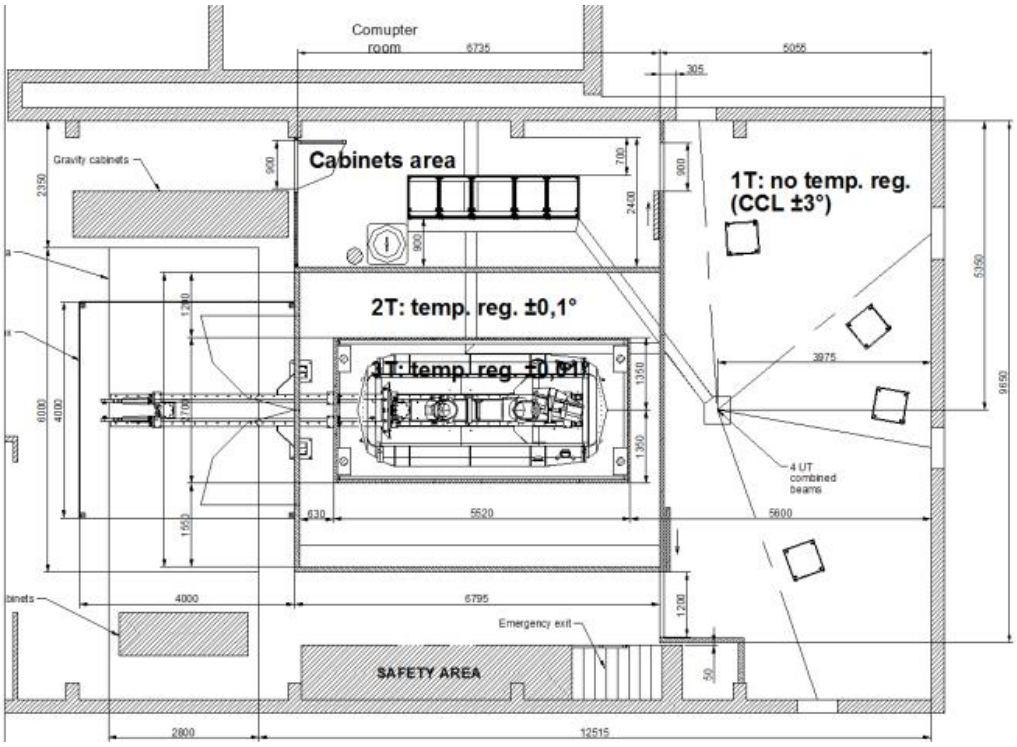

Figure 10: Schematic diagram of ESPRESSO inside the CCL, top view.

temperature control inside the cryostat head and its cooling system, as well as the thermal stability and the homogeneous dissipation of the heat locally produced in the CCDs during operations are of critical importance. For these purposes, ESO has built a new highly stable cryostat and performs continuous wiping and applies a custom read-out pattern to produce constant heat dissipation on the chips.

3.4 The Calibration Unit

The Calibration Unit (CU) includes a set of lamps and is connected to several calibration devices to properly calibrate the instrument. The lamp/devices lights can be fed into any of the two fibers ('object' or 'reference') and in each of the 4 FE. The FE unit injection system reproduces a calibration beam identical in diameter and F-number to the scientific beam from the telescope. When performing daily calibrations in 1-UT of 4-UT modes only one of the FE is fed the calibration light. Under regular operations, the FE-1 is used for daily calibrations for all the UTs in order to provide a common calibration reference.

These calibration lamps and devices provide i) the white light required for standard spectroscopic data characterization and reduction ii) wavelength calibration, and iii) radial velocity (RV) drift measurement. The sources are:

- A Laser-Driven-Light Source (LDLS) for order localization, profile definition, and spectral flat-fielding;
- A Thorium-Argon hollow-cathode lamp (ThAr) for absolute wavelength calibration under regular operations;
- A Fabry-Pérot (FP)-cavity illuminated in white light for simultaneous-reference (drift) measurements. This spectral lamp is also used in combination with the ThAr to extend

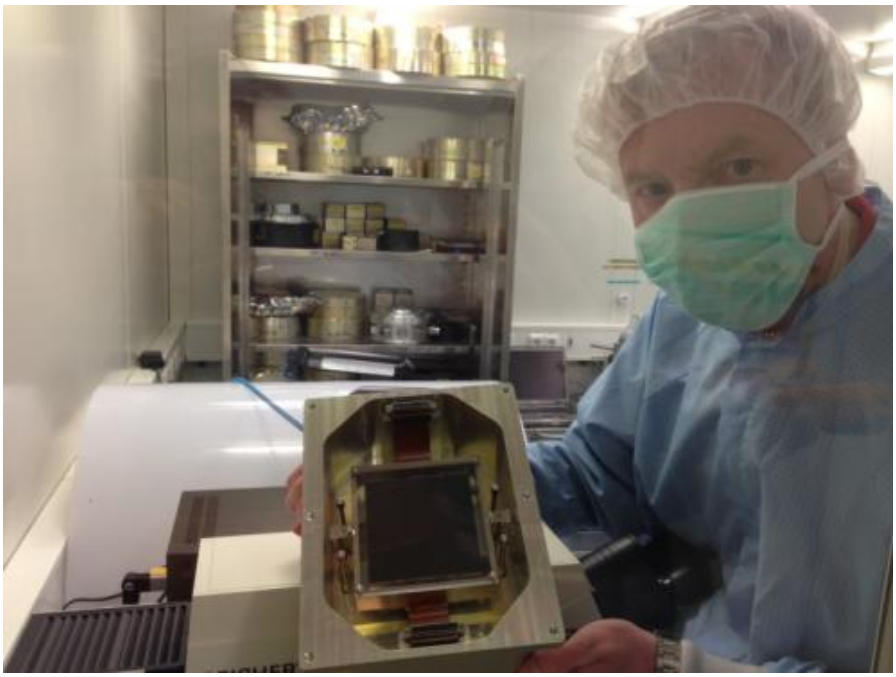

Figure 11: The first ESPRESSO e2v CCD in its shipping container, inside the ESO clean room.

and improve the wavelength calibration;

3.4.1 The Laser Frequency Comb

ESPRESSO is also equipped with a Laser-Frequency Comb (LFC), that has been developed by Menlo Systems. The system is designed to deliver the most accurate absolute (local) wavelength calibration (top level requirement of 10 m/s), which is needed for testing the invariance of fundamental physical constants, and for the redshift drift experiment (Sandage test). For this, the LFC produces a dense forest of equally spaced (in frequency) emission lines, which can be used to calibrate the instrument. The frequency of each individual line is given by the comb relationship: $\nu_n = \nu_0 + n \times \Delta\nu$, where ν_0 is the offset frequency, $\Delta\nu$ the repetition rate, and n is an integer number. Note that the current value of ν_0 is 7.65 GHz[2], and the (filtered) repetition rate corresponds to 18 GHz[3]. Figure 12 shows a schematic of the LFC main components and basic principles.

The ESPRESSO LFC was officially commissioned in October 2022. Unfortunately, soon after the LFC was put in operations, several problems affecting its availability, usability and performance have been detected. Among them, two main components were the most problematic ones. First, the original scrambling unit (SU; responsible for the light scrambling), was prone (by design) to damage the fibre (by the shaker motors inside the unit), leading to a rapid decrease in the light transmission, and subsequent irreversible damage of the fibre. In fact, the plastic fibre inside this unit, had to be replaced a couple of times. For this reason, the ESO Telescope and Instrument Optics group designed a new SU, which is more robust and with better scrambling properties. This new unit has been already tested and finally installed and

[2]This value is saved in the fits file header (INS5.LAMP4.FREQOFFS), and can be changed (it was 7.4 GHz until 2025).

[3]This value corresponds to the transmitted mode spacing (by the FP cavities), while the intrinsic comb repetition rate corresponds to 250 MHz

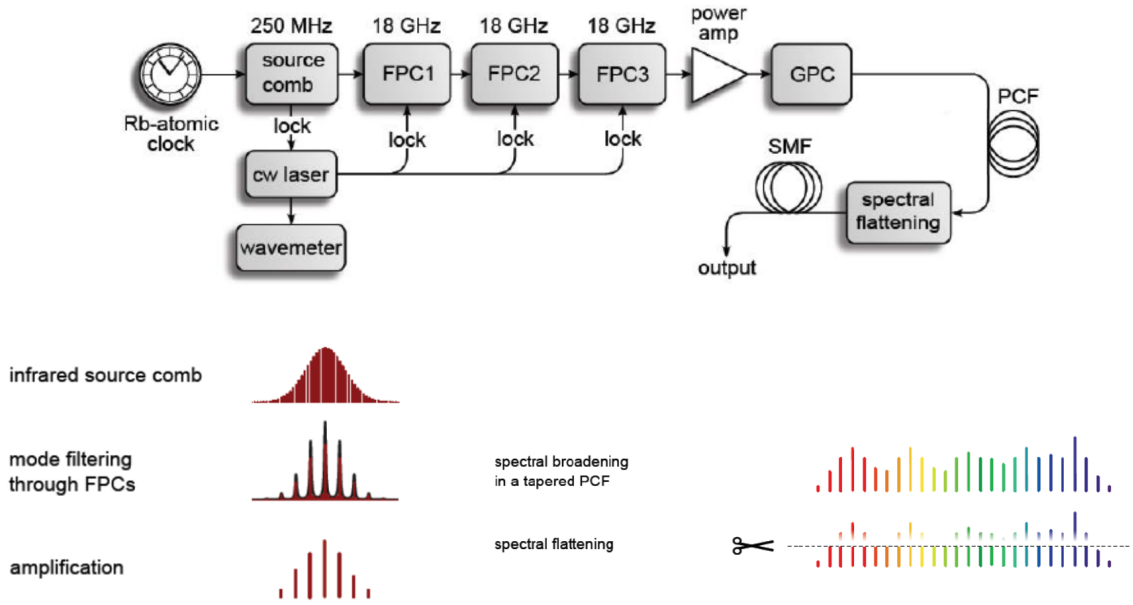

Figure 12: Schematic of the LFC including the main elements and working principles. Credit: Menlo System AstroComb Manual (Manual FC1000 - Astro v2.0)

integrated to the ESPRESSO LFC on April 2026. On the other hand, the original Blue-Sky photonic crystal fibre (PCF; See Fig. 12) responsible for the spectral broadening, was found to be intrinsically unstable, and introducing a high level of stochastically varying background, strongly affecting the quality of the data and the resulting wavelength solution. After many attempts to improve the long-term stability of the system, the ESPRESSO IOT decided to replace the Blue-Sky PCF by an Oscar-type PCF. The new system was extensively tested on August 2025, showing a massive improvement in the overall performance, both in terms of flux and wavelength stability. The main drawbacks of the new system configuration are: i) a slight reduction of $\sim$ 30 nm in the blue wavelength coverage (new blue cut-off $\sim$ 450 nm), and ii) a reduced lifetime of the PCF of the order of months[4], which is explained by the much higher power injected in the current LFC configuration. The new and final configuration of the system was performed on Nov 2025, and the LFC was officially put back in operations (for scientific use) on Nov. 21, 2025. Figure 13 shows an example of the local wavelength accuracy that can be reached in the current configuration (new PCF and SU). The measured median local wavelength accuracy is 5.8 m/s (in slice 1). Note that these results were obtained by a custom code developed by M. Jones (ESPRESSO IS), since the ESPRESSO pipeline does not fit the diffuse background of the LFC lines. An upcoming pipeline version will include this upgrade. Finally, a detailed description of the LFC, including the most relevant changes, tests and results will be presented by the ESPRESSO IOT in a forthcoming paper.

[4]In fact the first PCF installed in Nov. 2025, which was extensively tested, showed rapid signs of degradation after $\sim$ 3 months, it was already replaced by a spare one

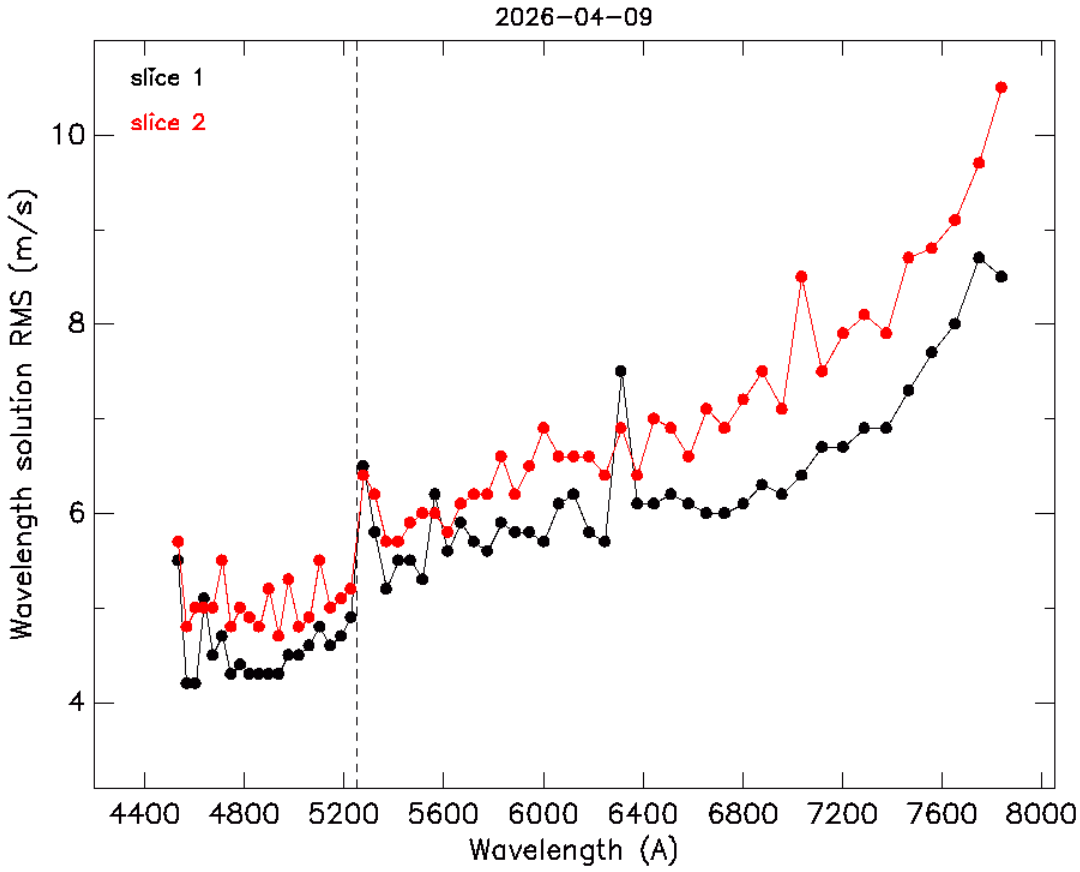

Figure 13: RMS of the LFC wavelength solution as a function of wavelength, from a spectrum taken in April 2026, with the new SU and PCF. The red and black points correspond to the slice 1 and 2, respectively. The vertical dashed line corresponds to the separation betwene the blue and the red detector.

Parameter/Mode	singleHR (1-UT)	singleUHR (1-UT)	multiMR (4-UT)
Wavelength range	380-788 nm	380-788 nm	380-788 nm
Measured Resolving power	140 000	meas. 190 000	70 000
Aperture on sky	1.0″	0.5″	4x1.0″
Spectral sampling (average)	4.5 pixels	2.5 pixels	5.5 pixels, binned x2
Spatial sampling per slice	9.0 or 4.5 pixels	5.0 pixels	5.5 pixels, binned x4
Number of slices	2	2	1 (merged)
Total efficiency	∼11%	∼5%	∼11%
RV precision requirement	10 cm/s	5 m/s	5 m/s
Measured RV precision	<20 cm/s	<1 m/s	<1 m/s

Table 1: Main Characteristics of ESPRESSO different Instrument Modes, taken from instrument specifications and latest health check measurements.

4 Configuring ESPRESSO

ESPRESSO was built for mechanical stability. By construction, the spectral format is fixed and the instrument configuration pre-defined. The three aspects in which a user can configure ESPRESSO for a science objective are:

- selection of the instrument mode, defining simultaneously spectral resolution, angle subtended in the sky and numerical sampling;
- selection of the source to illuminate the reference fiber;
- definition of the detector readout mode and associated binning.

The choices on these are interconnected, but for the sake of clarity are discussed separately.

4.1 Instrument Modes

The instrument mode defines the UT light feeding, 1UT vs 4UT, and for the case of 1UT the selection of the fiber size to use: 1″ for HR (High-resolution) *vs* 0.5″ for UHR (ultra-high resolution). ESPRESSO was designed to operate in the slit-limited regime of resolution, i.e., the spectrograph's resolution will depend on the slit width on the direction of main dispersion. When collecting light from 4UT the fiber image seen by the spectrograph is the bundle of four 1″ fiber; it is thus wider and the resolution is then necessarily lower, being called MR (medium resolution).

ESPRESSO provides then three instrument or observing modes: singleHR, singleUHR, and multiMR. The main characteristics of each observing mode are summarized in Table 1. For daily updated values on the main key performance indicators, please refer to the ESO Health check page.

The singleHR mode was developed for the measurement of precise RVs. It delivers a very high spectral resolution while maintaining a high overall transmission, two key factors for the measurement of precise RVs, as seen in Section 2.1. The singleUHR mode employs a fiber with half the diameter on the sky, attaining higher spectral resolution – and for resolved Solar System objects, higher *spatial resolution* – at the cost of increased slit losses.

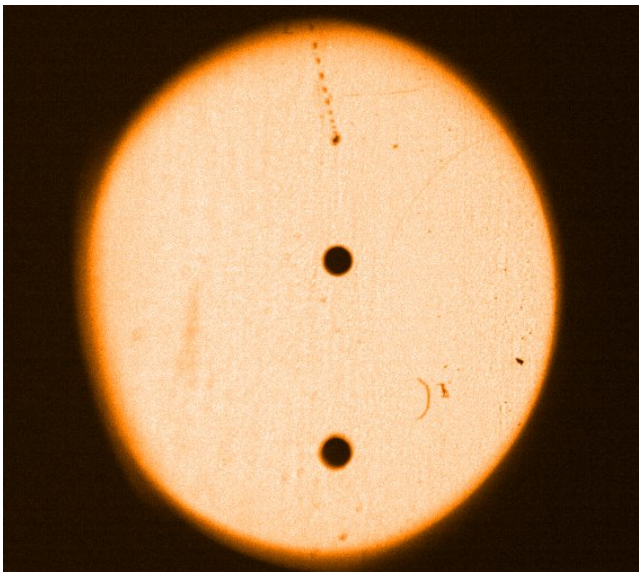

Figure 14: ESPRESSO Instrument FoV illuminated by an homogeneous source. *If you tilt your head sideways to the left, you can see ESPRESSO smiling back at you.*

The multi-MR mode was designed to exploit the full collecting power of using simultaneously the 4UT. It is best suited for very faint objects or transient ones in which an extremely high S/N is required on a very short integration time.

4.2 Source on the reference Fibre

The reference fibre can receive either sky light or light from a calibration source for simultaneous instrumental drift measurement.

In the first case, the reference fiber collects sky light from a second pinhole that points to a distance of $7''$ away from the main scientific target. The instrument's FoV is approximately elliptical, due to light blocking by several optical devices (and their covers) as the light travels along the Coudé Train. These two properties are noticeable in Fig 14. As the field rotates, the stellar coordinates to which the pinhole point to change with time, and care must be taken by the user when collecting skylight on a crowded field to make sure no star falls in the pin-hole.

Alternatively, a source can be used to illuminate the reference fiber at the same time we collect scientific data on the object fiber. This option is used to track instrumental drifts down to the cm/s level. The mode was developed for high S/N scientific exposures; when calculating the RV on these the limiting factor is not the photon noise on the target but potential instrumental drifts inside the spectrograph.

For high RV precision, at the level of m/s or better, the usage of simultaneous drift reference is recommended. This is only necessary when the photon noise reached on the target is of the same level or smaller, otherwise photon noise on the target will be the limiting factor.

For RV targets with a photon noise larger than 1 m/s, targets for which no RV measurements are intended, or for sources for which a high spectral fidelity is preferable rather than tracking the instrument's internal drift, it is preferable to use the reference fibre to measure the sky spectra. By doing so one can characterize accurately the sky background and the detector noise contribution to the error budget. When pointing the fiber B to the sky the user should make sure that no companion star falls on it during the course of observations.

Detector Mode	Binning (spat. x disp.)	Read-out speed	RON (Blue/Red)	Conversion factor	Read-out ports	Read-out Overheads
FAST	1x1	500 kpx/s	8 / 5 [e-/pixel]	1.1 [e-/ADU]	2x8	45s
SLOW	2x1, 4x2, 8x4	100 kpx/s	3 / 2 [e-/pixel]	1.1 [e-/ADU]	2x8	68s, 41s, 36s

Table 2: ESPRESSO detector modes and associated overheads.

Binning	X	Y	Pre-X	Over-X	Pre-Y	Over-Y
1x1	1152	4616	24	64	0	32
2x1	576	4616	12	32	0	32
4x2	288	2308	6	16	0	16
8x4	144	1154	3	8	0	8

Table 3: Frame Size as a function of binning scheme on each individual read-out port.

4.3 Detector Readout Modes

The scientific detector allows for different read-out configurations optimized for either low or high-S/N measurements. For high S/N measurements, when the read-out noise (RON) does not contribute significantly to the error budget, 1x1 pixel binning is offered to provide faster read-out and maximize the duty cycle (open-shutter time). On the other hand, for low S/N measurements detector RON can contribute in a significant proportion to the error budget. For these cases a 2x1 binning factor, with binning in the spatial direction plus a slow read-out is used to minimize noise contribution. Given the usually long exposure times used on faint targets, the longer readout time of this configuration does not impact significantly on the duty cycle of the observations.

The fast readout mode (1x1) shows an electronic correlated noise pattern at the level of the read-out-noise, and as such it is strongly discouraged for faint targets.

The total overheads contain the time spent on readout, transfer, and wiping operations and are listed for each of the binning and readout schemes in Table 2.

The active area of each of the two detectors consists of 9216 optically active pixels in the spatial direction or cross-dispersion direction (X), and 9232 optically active pixels in the main dispersion direction (Y). The Echellé orders are thus aligned along the CCD columns (Y). The detector is read out through 2x8 ports, dividing the raw frames in 2 sections along Y and 8 sections along X. Table 3 indicates the raw-frame size provided by each individual read-out port after binning. Pre- and over-scan regions are produced in a symmetric way for each read-out port. The spectrum is assembled into a single FITS file containing two raw frames composed each of 2x8 individual sub-frames aligned according to the physical layout but separated by the pre- and over-scan regions of each sub-frame. The dimension of the images will naturally depend on the used binning.

4.4 Instrument configurations

By putting together the different options described above we have the instrument configurations available for different scientific goals, listed in Table 4.

The science case (and to some extent the faintness of the target) will define the observing mode: singleHR, singleUHR, and multiMR. The readout and binning options in singleHR and multiMR should be chosen by comparing the options' relative merits.

Observing Mode	Broad Scientific Goal	Templates	RO mode	Det. Binning
SINGLE_HR11	Spectroscopy and RV monitoring at high S/N with 1UT	singleHR	FAST	1x1
SINGLE_HR21	Spectroscopy and RV monitoring at medium or low S/N with 1UT	singleHR	SLOW	2x1
SINGLE_HR42	Spectroscopy at low or RON-limited S/N with 1UT	singleHR	SLOW	4x2
SINGLE_UHR11	Very high-resolution spectroscopy with 1UT	singleUHR	FAST	1x1
MULTI_MR42	Spectroscopy of faint targets with 4UTs	multiMR	SLOW	4x2
MULTI_MR84	Spectroscopy of faint targets with 4UTs	multiMR	SLOW	8x4

Table 4: Summary of ESPRESSO's instrument configurations.

- FAST 1x1 vs SLOW 2x1 vs SLOW 4x2 (in singleHR): The choice here is between reading faster and introducing an electronic pattern or reading slower with a lower read-out noise (RON), and potentially lower sampling. For exposures with S/N $\geq$ 100 we are photon-noise dominated, and the difference in RON between the two modes will be negligible. In these cases FAST 1x1 allows a (slightly) faster readout without a negative impact on the science. For S/N<100 the users should check if they prefer the lower noise provided by SLOW 2x1 or the shorter overheads provided by FAST 1x1. For very low S/N the RON contributes significantly for the error budget. In these cases the integrations are often long, and observing in SLOW 2x1 allows for a higher S/N while having a negligible impact on the total time on target. In RON-limited cases, or simply if the user privileges S/N over numerical sampling of the features, SLOW 4x2 can be used (see Berg et al. 2022). Therefore the HR 4x2 mode should not be used for precision RV studies.

- SLOW 4x2 vs SLOW 8x4 (in multiMR): This choice should consider 3 different aspects: the sampling in dispersion direction, the RON value, and the overheads. The user should weight observing at higher sampling with longer (read-out) overheads, with observing at a lower sampling but with shorter overheads and lower RON. Since these modes are mostly used on faint targets, the integration times are long and the overheads have little impact on the total time on target. It becomes then a matter of weighting the gain on S/N provided by SLOW 8x4 with the gain in sampling provided by SLOW 4x2.

Please refer to the ESPRESSO ETC for an informed S/N comparison on using the different modes.

The spectrum is spread over two CCDs, the blue- and the red-arm detectors, which cover the spectral ranges of 380-525 nm and 525-788 nm, respectively. For a detailed description of the spectral format the reader is referred to Appendix A.

Due to the presence of the APSU, for the singleUHR and singleHR modes each order is composed of two slices with the same spectral information content but recorded on different physical pixels. For the multiMR mode there is only one slice, created by the dispersed image of the square fibre bundle.

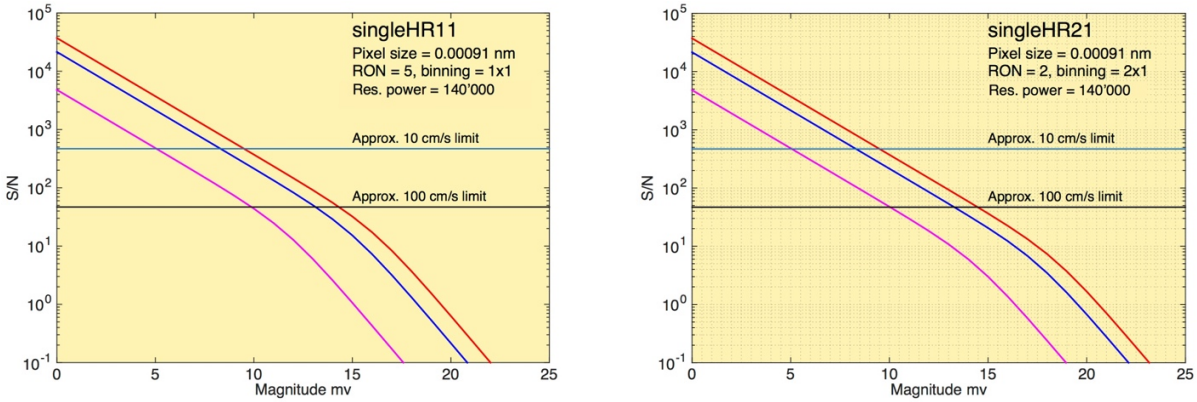

Figure 15: S/N vs. stellar magnitude for *singleHR11* and *singleHR21* configurations for exposure times of 60 s (pink), 1200 s (blue) and 3600 s (red). The slope change defines the magnitude at which the measurement becomes detector RON limited. S/N for 10 cm/s and 100 cm/s are shown. The values are estimated for slowly-rotating, inactive late-G or K dwarf stars, calculated for a seeing of 0.8″ and an airmass of 1.

5 Instrument performance and known issues.

5.1 Total Efficiency and on-sky RV precision

The different fiber diameter, readout noise and pixel binning lead to a different S/N ratio per extracted pixel for the different modes. The approximate S/N for the five offered setups is shown in Fig. 15, Fig. 16, and Fig. 17. For reference, on an exposure of 60 s on a V = 8 star with a seeing of 0.8″ and at an airmass of 1, on singleHR mode we reach a S/N of about 100 per extracted pixel. This translates to a photon-noise RV precision of approximately 50 cm/s for a non-rotating, inactive K5 dwarf star. For earlier type stars and/or rotating stars, the internal RV precision will be lower at equal S/N, as consequence of the lower line density and wider lines. The difference in S/N between the *singleHR11* and *singleHR21* instrument configurations will only be apparent at faint magnitudes when the detector RON starts to dominate. The singleUHR mode has lower total transmission due to larger slit losses, a price to pay for the higher resolution. On Fig. 17 we notice the gain in S/N achievable by using the mode multiMR. The factor of 2 comes from the larger collecting area of the 4 UTs when compared to a single UT. An additional factor of sqrt(2) or 2 is also obtained thanks to the binning by 2 or 4 pixel in the spectral direction in the *multiMR42* and *multiMR84* configurations, respectively. The gain in choosing a large binning factor is evident in low S/N regime and increases closer to the limiting magnitudes, at which the observations are RON limited. This represents the main advantage of the ESPRESSO 4UT mode against four equal exposures in single-UT mode obtained sequentially. For reference, in multiMR 8x4, we can achieve a S/N per extracted pixel of about 15 at 550 nm on a V = 19 target in a single 1-hour exposure.

Different instrument configurations show a relative RV offset, as expected due to the properties of each setup (i.e., different spectral resolution and/or binning). The RV offsets are of ∼2 m/s between HR11 and HR21, and of ∼20 m/s between UHR and HR21 or MR42 and HR21. These values are to be taken as illustrative, as they will depend on the characteristics of the target and of the RV calculation. The user is strongly recommended to stick to the same observing mode for a given science case (i.e., for a given target and science goal).

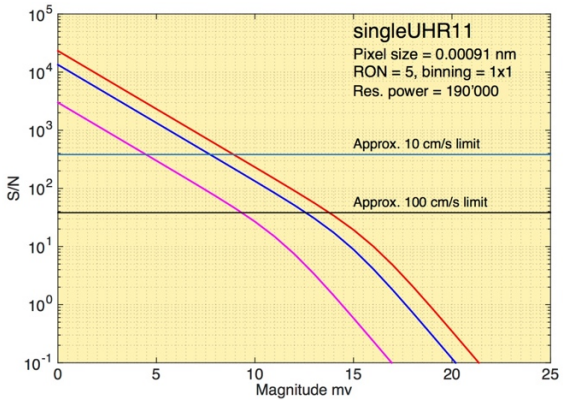

Figure 16: Same as Fig. 15 but for the singleUHR configuration.

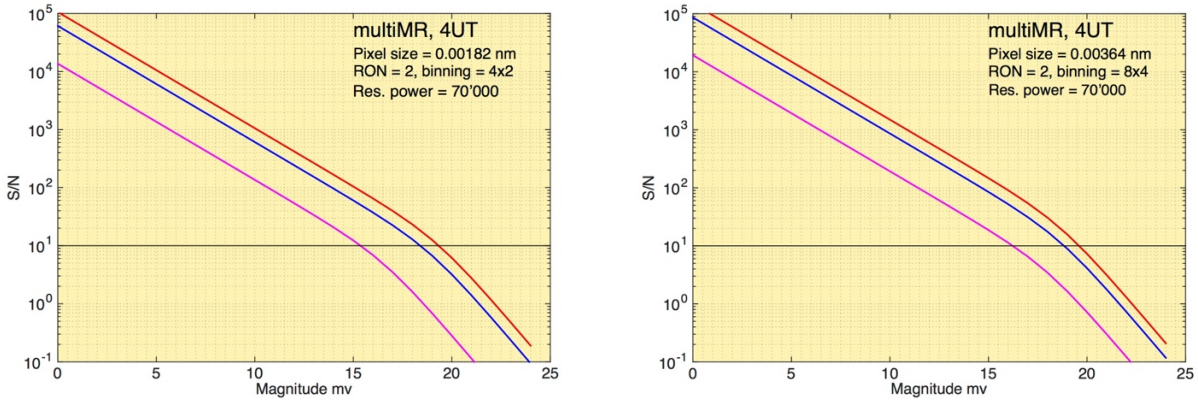

Figure 17: Same as Fig. 15 but for the *multiMR42* and *multiMR84* configurations.

The RV precision of ESPRESSO has been measured to be very close to the goal of 10 cm/s. Long sequences of observations in the HR mode show a precision of better than 15 cm/s on the short term (i.e., within one night). The instrument can reach photon-noise limited uncertainties at the level of 10 cm/s in photon-noise-limited (i.e., high SNR) spectra of G and K-type stars. In the MR mode, a precision better than 1 m/s can be achieved over a few hours. On UHR mode, the main practical limitation is the larger photon noise incurring from still losses, leading to lower precision than in the HR mode. However, UHR is not expected to deliver a higher RV precision than HR due the stellar $v.\sin i$ becoming the limiting factor on the final FWHM.

It is important to remember that to reach a precision of the level of 1 m/s or better, it is necessary to use a simultaneous drift reference. As detector cryostat stability improves, in the near future it will be possible to reach this precision value without using simultaneous reference.

5.2 Dark Current, Diffused Light, Ghosts, and Sky Background

The dark current measured on the ESPRESSO CCDs is of the order of 1 e-/hour/pixel. Dark frames are taken periodically as part of the long-term calibration plan for monitoring of the detectors' dark current.

Scattered light is the diffuse component of the inter-order contamination measured on the CCDs; it is proportional to the total flux received in the focal plane and varies smoothly across the detectors. A maximum diffuse background below 0.1% of the peak flux has been measured. Only for very blue targets a larger diffuse background has been measured on the extreme blue part of the spectrum.

Ghosts are parasite orders that exist in grating spectrographs (due to the high number of optical components) and cannot be avoided. In ESPRESSO, ghosts are extremely weak; they are only detectable when exposing with the ThAr lamp, that exhibits extremely strong Argon emission lines. No ghosts have been sighted on science exposures.

When observing in simultaneous reference mode (see Fig. 18), direct contamination from the FP light used in the reference fibre (Fibre B) can pollute the spectral orders of the object fibre (Fibre A). This contamination is smaller than 10^{-4} of the FP light, but for faint targets may correspond to a large fraction of the total science target flux at a given wavelength. Since for faint targets sky subtraction is essential, it is recommended not to use the simultaneous reference technique for targets fainter than V = 12, but rather record the sky spectrum in Fibre B (simultaneous-sky mode). The pipeline will automatically subtract the sky background from the object spectrum when observing in this mode.

5.3 Interference pattern introduced by the Coudé Train

ESPRESSO spectra are affected by two different interference patterns induced by coudé train optics. Approximately sinusoidal "wiggles" become apparent when spectra taken in different telescope positions are divided by each other, although they are also present and detectable in the individual frames. The first set of wiggles has a period of 30 Å at 600 nm and an amplitude of ∼1%. In contrast, the second set of wiggles has a shorter period of 1 Å at 600 nm and an amplitude of ∼0.1%. For a detailed analysis, the user is referred to section 3.4 of the PhD thesis by Romain Allart. Some examples of such wiggles reported in scientific studies include Allart et al. 2020, Sedaghati et al. 2021 and Casasayas-Barris et al. 2021. The consortium

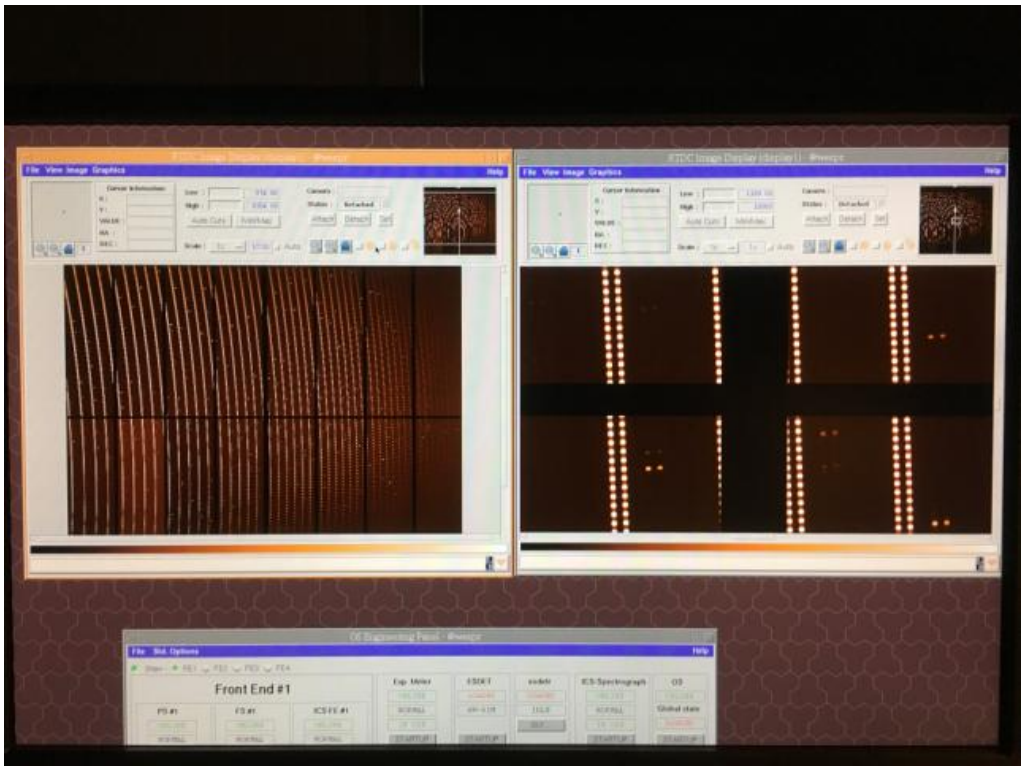

Figure 18: Example of raw frame plus zoom in, on the right-hand side, from the red CCD of ESPRESSO illuminated with the ThAr lamp (in Fibre A, to the right) and the Fabry-Pérot simultaneous calibration light (Fibre B; continuous dots to the left).

and ESO are working together to characterize this effect.

5.4 Blue Cryostat Temperature instabilities (before May 2022)

While the red detector's RV precision was at the $\sim$ 10 cm/s level, the blue detector variability was as large as $\sim$ 60 cm/s for intervals of a few minutes. A Fourier analysis of RV drift calculated on calibrations time series of several hours shows strong periodicities at 5 and 7 min, that are responsible for a fraction of the RV variability found.

A preliminary analysis of the spare cryostat in Garching showed that a badly fixed temperature sensor could introduce a temperature oscillation that will then propagate to the detector, explaining what is observed on ESPRESSO data. This problem was solved during a highly invasive instrument intervention that took place on May 2022 (see section 6). However, all of the ESPRESSO data taken before that time are affected by this problem, and thus the RV precision achievable in the blue detector was of several dozens of cm/s, ultimately depending on the integration time and how the effect is averaged out.

Between the 28th of April and the 2nd of May 2021, a malfunction of the nitrogen feed of ESPRESSO's blue cryostat introduced a temperature oscillation that propagated down to the detector. While the instrument is usually closely monitored and the issues timely corrected for, the very low staffing of the Observatory during COVID pandemic allowed this problem to pass unnoticed. As a consequence, the blue cryostat internal RV daily drift, that is usually within 2-3 m/s, degraded to approximately 10 m/s during this short period of 5 days.

We advise special caution on the interpretation of RVs derived using blue cryostat spectra. The drift methodology was not devised to correct drift values much larger than 1 m/s, and

for drifts of ∼10 m/s the error on the blue RVs, after correction, can still be of the order of 1 m/s. We recommend checking the value of the drift calculated on the blue detector by using the blue detector drift value

HIERARCH ESO QC DRIFT DET0 MEAN = 0.00218304501626747 / mean drift [pxl] for det

and multiplying this by 480 m/s (the size of a pixel in RV). If this value is larger than 2-3 m/s the data is affected beyond the typical cryostat instability issue.

5.5 ADC/PLC issues on Jan-Apr 2021

From January to April 2021, ESPRESSO was affected by critical software issues. These low-level issues, at the level of communication with the Programmable Logic Controller (PLC), did not trigger any error or warning. The problem thus compromised a large number of observations for several programs before it was identified. It was originally misdiagnosed as an UT2 ADC2 failure, while further investigation showed that it resulted from a pure communication issue affecting the four ADC2's. It affected thus data on each of the UTs in a similar way.

The faulty data can be identified by the absence or zero value of the header keywords

HIERARCH ESO INS ADC2 RA = 0. / [deg] Telescope right ascension.
HIERARCH ESO INS ADC2 SENS1 = 0. / [mbar] Pressure.
HIERARCH ESO INS ADC2 TEMP = 0. / [C] Temperature.

With ADC2 being non-responsive, the atmospheric dispersion was not corrected for, and the chromatic stellar images formed on the field-stabilization TCCD did not overlap spatially. This introduced a wavelength-dependent light loss at the fiber interface.

A comparison of RV datasets taken with the ADC operating in and out of range, i.e., correcting all atmospheric dispersion or leaving uncorrected atmospheric dispersion, respectively, shows that the latter dataset is affected by an additional scatter of the order of 1 m/s. A faulty ADC will not correct or even introduce an atmospheric dispersion having an effect that is, to first order, similar to having an ADC operating out of range, and thus of the same order of magnitude (see Fig. 19).

An important exception applies. The ESPRESSO pipeline was devised to correct the residual atmosphere dispersion effect, i.e. after ADC correction. This reduces significantly the chromatic effects on data. If flux correction is possible, i.e.

HIERARCH ESO QC SCIRED FLUX CORR CHECK = 1 / Flux correction QC

then the impact remains at ∼1 m/s. If this quality control (QC) did not pass, having the value of 0, the flux correction was not applied and the effect can be of several m/s.

Finally, programs aiming at high spectral fidelity will be compromised by systematic errors on the flux and line-spread function determinations. The severity of these effects will vary from

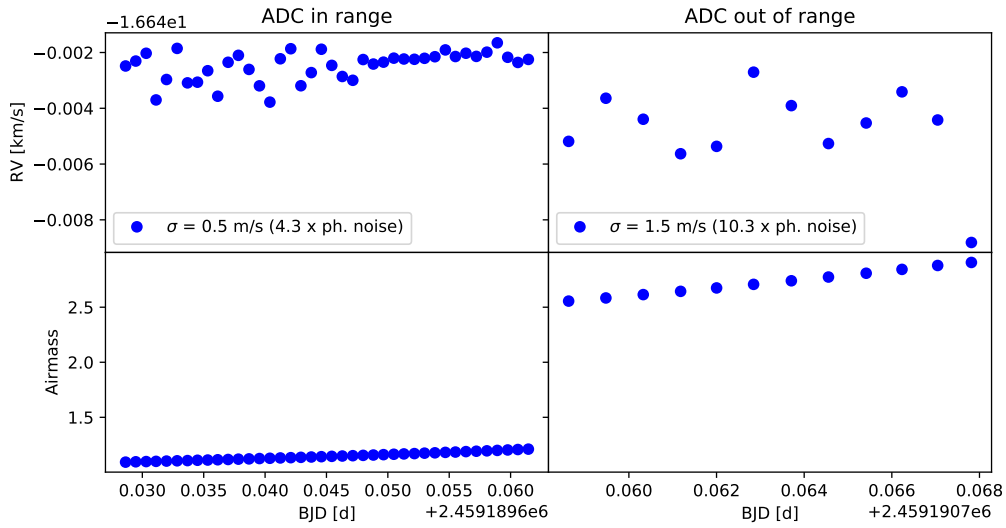

Figure 19: Example of the effect on the RV of an ADC opening in (*left*) and out (*out*) of airmass range.

spectra to spectra. Without a precise knowledge of the ADC2 true position, they are very difficult to correct.

5.6 Exposure meter de-synchronization (Oct. 2021 to Aug. 2023)

A VLT software (SW) upgrade on October 2021 led to an unexpected de-synchronization between the exposure-meter (EM) and the science detector, resulting in a $\sim$ 8-10 seconds delay of the EM starting time, after the shutter in the science detector opens. This issue thus affects the flux-weighed exposure central-time, and hence the computed barycentric correction. One example of this issue is presented in Figure 20. After identifying the problem, a software patch was installed in August 2023, which solved the problem. The delay is now < 2 seconds, as was the case before the VLT SW upgrade. Finally, this new patch also removes negative time values in the EM tables, that were present in some files. We note that the ESPRESSO pipeline (since version 3.0.0) removes the negative time stamps in the EM tables.

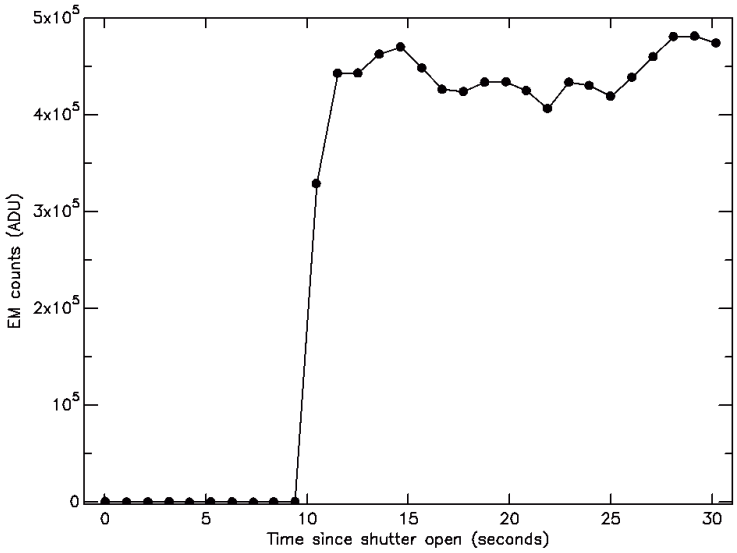

Figure 20: Exposure meter table for an observation affected by the EM de-synchronization. It can be clearly seen that the EM does not record any flux in the first $\sim$ 9 seconds of the exposure.

6 Detector's cryostasts repair intervention

The activities were performed in the context of the cryostats repair and detectors activities, aimed at improving the instrument stability and overall performance. The intervention took place between May 1st and May 15th of 2022. Here are a summary of the main activities done:

- Repair and reassembly of the blue and red cryostats, including fixing all temperature sensors, decoupling the mechanical link between the cold finger and the detector mount, adjustment and verification of the temperature control loops. These activities were performed mainly to improve the stability, particularly on the blue side.
- Replacement and validation of the Front End Boards in the NGC systems, addressing the quantization issues noticed especially in the fast readout mode, and implementing the correct synchronization in the NGCs systems
- Fix and validate read-out noise performance, especially in the blue detector.

Below is a summary of the main results after the intervention:

6.1 Spectral format

After the intervention a small shift of the line and orders position was found, in both x- and y- direction (cross-dispersion and dispersion direction, respectively) and in both the red and blue detectors. By looking at individual ThAr lines, their centroids in the red detector moved by around -0.5 [pix] and -1.1 [pix] in x- and y- direction, respectively. Similarly, in the blue detector they moved by around +1.6 [pix] and -1.6 [pix] in the x- and y- direction, respectively. Given that these shifts are relatively small, the ESPRESSO pipeline version 2.3.5 was able to

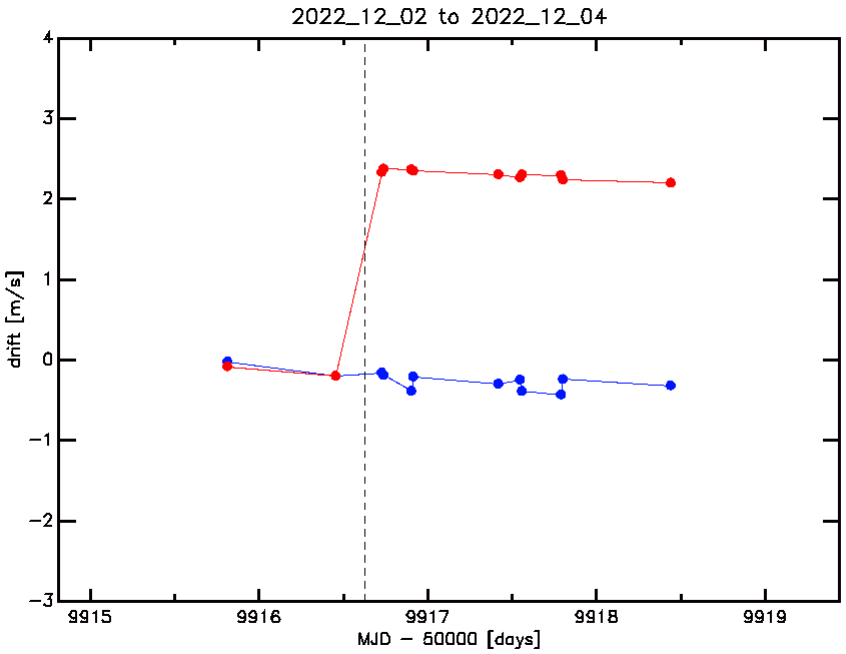

Figure 21: RV drift computed from FP-FP data taken between 2022-12-02 and 2022-12-04. The blue and red dots correspond to the blue and red detectors, respectively. The vertical dashed line shows the time when a micro-earthquake close to Paranal happened.

properly reduce the new HR1x1 and HR2x1 data. However, for the HR4x2 and MR4x2 mode the pipeline crashes when computing the FP wavelength calibration. This fix was already implemented in the pipeline version 2.4.0 and propagated into the newer versions.

6.2 Instrumental stability

To assess the internal short-term instrumental stability, several Fabry-Perot (FP) sequences were obtained after the instrument was closed and stabilized (for more than a week), which were used to compute the instrumental drift. The results are presented in Figure 21. As can be seen, there is a significant improvement in the drift stability in the blue CCD after the intervention.
Similarly, several spectra of the RV standard star HD85512 were collected before and after the intervention aimed at studying any potential RV offset between pre- and post-intervention data. Figure 23 shows the resulting RVs for the HR1x1 and HR2x1 modes. As can be seen there is no obvious RV offset between pre- and post-intervention data. However, further data and a more detailed analysis is needed to properly characterize any potential (chromatic) offset.
Finally, the ESPRESSO IOT has noticed that the occurrence of micro-earthquakes in Paranal can lead to large RV drift values (at the $\sim$ 1-5 m/s level), mainly in the red detector. This is indicative that the red cryostat is more sensitive to vibrations than the blue one. We can also confirm that this is present only in the data taken after the intervention in May 2022. An example of this is presented in Figure 22. As can be seen, there is a sudden jump in the drift in the red detector after the micro-earthquake, while the blue one is not affected. A more detailed investigation to quantify this effect is underway, and the final results of the analysis will be available to the ESPRESSO users in the upcoming version of the UM.

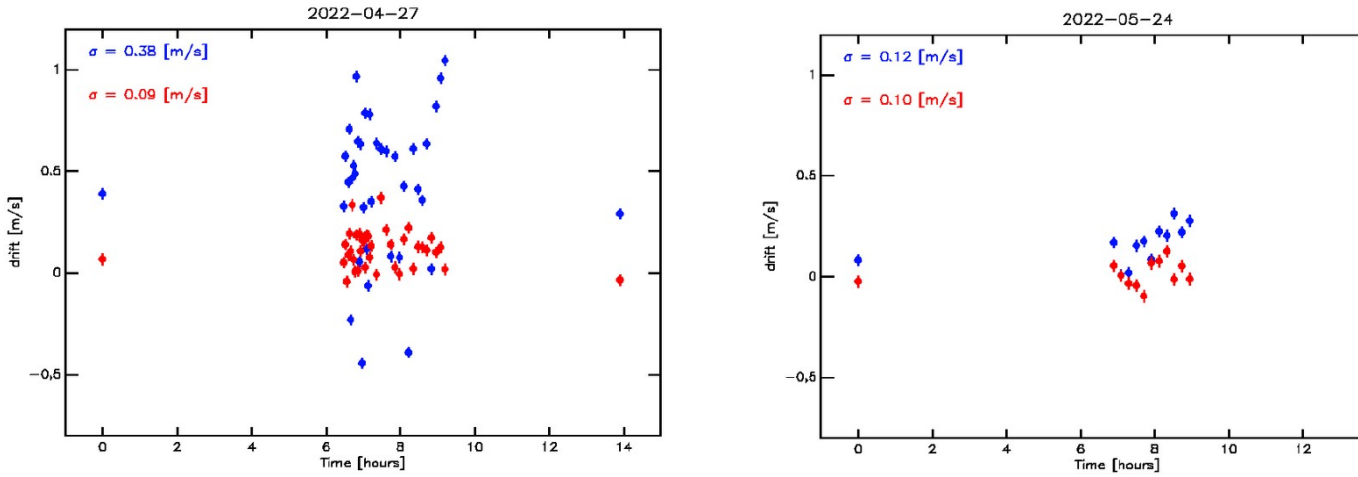

Figure 22: RV drift computed from a FP-FP sequence taken before and after the intervention (left and right panel, respectively). The blue and red dots correspond to the blue and red detectors, respectively. The corresponding values of the RMS are also labelled.

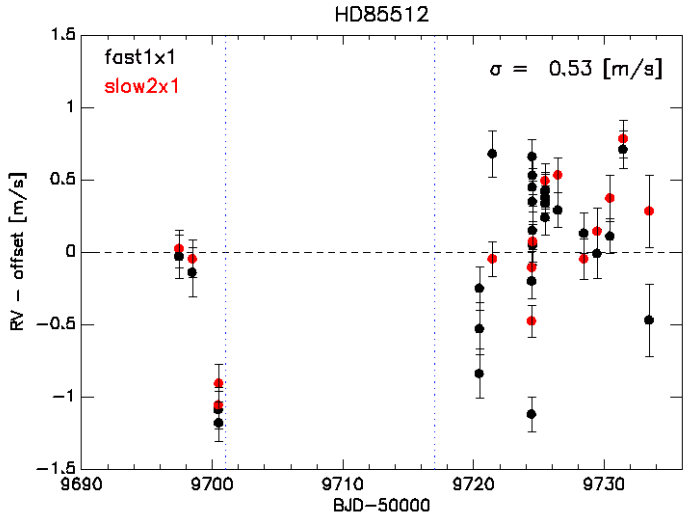

Figure 23: Radial velocity variations of HD85512 as a function of time, for the HR fast 1x1 and slow 2x1 read-out modes (black and red dots, respectively). The blue dotted lines mark the beginning and end of the intervention.

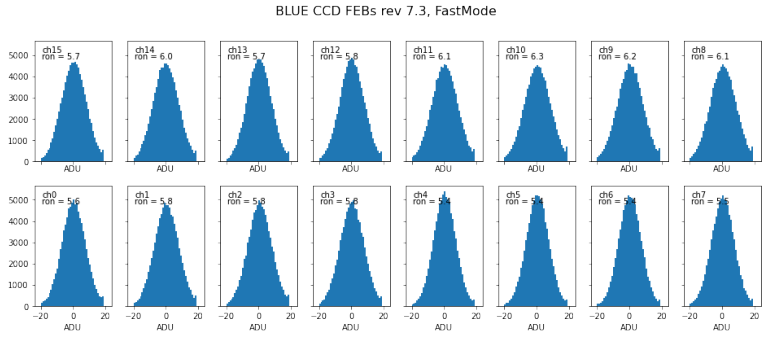

Figure 24: Blue CCD histograms with FEBs revision 7.3.

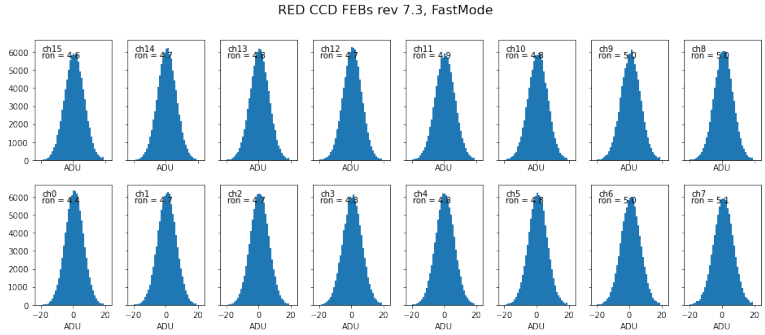

Figure 25: Red CCD histograms with FEBs revision 7.3.

6.3 Replacement of the NGCs front end boards

The ESO NGC team and the detector group completed an intense work to fix the quantization issues (missing bits) noticed in the FEB board 5. The histograms presented in Figures 24 and 25 demonstrate that the original missing bits on ADC for FEB boards 5 is not present on the new FEB boards 7.3. All the channels on both the Red and Blue CCDs do not show missing values and the shape is Gaussian.

7 Observing with ESPRESSO

From the operational point-of-view, ESPRESSO is a relatively simple instrument, with a fixed spectral format and five well-defined instrument configurations to select from; these correspond to the possible combinations between HR, UHR, MR and the different binning+readout schemes (see Table 4). Since Period 102, ESPRESSO has been offered for service and visitor mode operations in 1UT mode. The 4UT mode of ESPRESSO has been offered in visitor mode since Period 103.

Once the instrument configuration is defined, the only remaining set-up choice is the light source illuminating Fibre B, the reference fiber. The available options are FP for simultaneous drift measurement or the SKY for sky recording and. The FP source must be used if the highest RV precision is required (at m/s or better). For relatively faint targets (V>12), the contamination of the science spectrum by the simultaneous reference source (at 10^{-4}) can be a limiting factor. In this case the RV precision will be dominated by photon noise on the target, and it is recommended not to use the simultaneous reference source, but rather to record the sky and background spectrum in Fibre B. If one aims a precision of 1 m/s on a V>12 target,

a choice must be made between highest RV precision and accurate sky subtraction.

ThAr and LFC frames are taken during daytime to provide the absolute wavelength calibration and none of them are taken during the night. Therefore they cannot not be used neither as simultaneous calibration, nor as an attached calibration before/after a science OB.

Just like for other ESO instruments, the preparation of ESPRESSO observations is done with *p2* and assisted by the Exposure Time Calculator (ETC).

7.1 Using the ETC to prepare observations

The ESPRESSO ETC is available at:

http://www.eso.org/observing/etc/bin/gen/form?INS.NAME=ESPRESSO+INS.MODE=spectro.

The input form allows you to select:

- Target brightness, spectral and spatial distributions.
- Sky background, defined by moon phase and distance, and airmass. Sky brightness calculation is based on the Cerro Paranal advanced sky model; the previous parameters can be input directly or calculated from the target coordinates and moment of observation.
- Turbulence category defining the seeing value observed at 550nm at zenith; the calculator will provide the corresponding Image Quality (or the other way around) using a model of the atmosphere, telescope and instrument (see dedicated documentation for detailed documentation). An estimate of the probability of realization of the requested seeing is given upon selection.
- Instrument configuration and number of UTs feeding the instrument (either 1 or 4).

Output from the ETC includes a summary of the input configuration; results are given in two tables, one for each detector.

Slit losses are a strong function of astrometeorological conditions. When preparing SM observations, users should should make sure the S/N required is achieved for the observational constraints specified in the OBs, while having the flux measured on the detector below the linearity limit (55 ke-). In particular, for singleUHR OBs with loose IQ constraints, the user should be aware that the OBs can be observed under much better conditions. For singleUHR OBs, it is good practice o include in the README the optimal integration time for the median seeing of Paranal (∼0.8), for which the target S/N and science objective can safely be achieved.

7.1.1 Turbulence Categories and Constraints

Since P105, observing conditions are specified in the form of Turbulence Categories. These are defined as the conditions that satisfy a given percentile of the available observing time in Paranal. For non-AO instruments like ESPRESSO the only relevant turbulence parameter is the seeing, and these categories correspond to the seeing thresholds listed in Table 5.

The values above were computed using the cumulative distribution of the seeing, after applying a rolling 90th-percentile over 1h. For ESPRESSO OBs with a duration shorter than an hour,

T Category	10%	20%	30%	50%	70%	85%	100%
Seeing threshold	0.50″	0.60″	0.70″	0.80″	1.00″	1.30″	all

Table 5: Turbulence Categories for non-AO instruments.

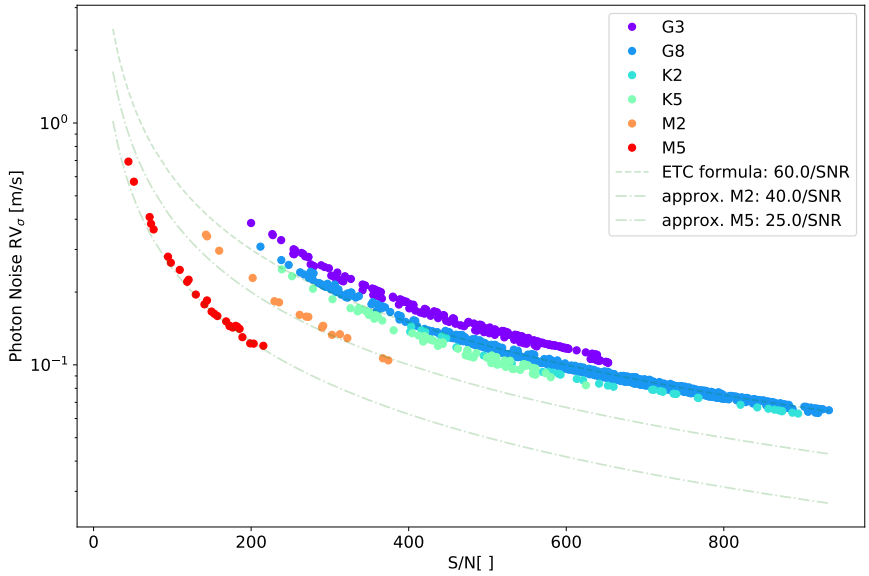

Figure 26: Photon noise as a function of S/N for for G2-M5 stars. Created using ESPRESSO GTO data, reproduced with the authorization of the PI.

the probability to satisfy a given seeing constraint is specified in the Turbulence category above. For updated information on the topic please refer to

https://www.eso.org/sci/observing/phase2/ObsConditions.html.

7.1.2 RV precision from the ETC

As we saw in Sect. 2.1, in the high S/N regime the RV precision depends linearly on S/N. If we assume that other parameters are held constant, one can then write $\sigma_{RV}^{-1} = a/(S/N)$ in which a is a constant to be determined.

The ESPRESSO ETC estimates RV precision using the formula $\sigma_{RV}^{-1} = 60/(S/N)$, calibrated using singleHR11/21 observations of non-rotating G and K stars. As can be seen from Fig. 26, this is a very good approximation. As one observes later spectral types, the precision increases, with a lower a. Two examples for two M2 and M5 stars are shown, but the reader should be warned that these are not necessarily representative of their spectral type. It is harder to find non-rotating Ms (as the ones depicted) than their G and K counterparts. Moreover, these stars can display strong stellar activity, an effect that adds up to the photon noise represented here. Moreover, this calibration assumes high S/N spectra, and may not be valid if S/N < 50.

7.2 Preparation of P1 and P2 material

During Phase 2, the successful applicant prepares their instrument set-ups and observing strategy through the elaboration of so-called Observation Blocks (OB) and related material.

An OB for a typical science observation with ESPRESSO consists of one acquisition template and one or several observation (integration) templates. The templates need to have the same instrument mode (e.g., singleHR or singleUHR).
For detailed instructions on how to prepare ESPRESSO OBs using *P2*, please refer to the ESPRESSO P2 tutorial.

7.2.1 Template parameters

The available templates, their parameters and options are described in detail in the ESPRESSO template manual. The instrument configuration defines the templates to use. Within a given template, one can find the following ESPRESSO-specific choices:

Acquisition template:

- Object V mag, used by the Instrument Operating System to define the integration time of the technical CCDs, used for target acquisition, field stabilization and Exposure Meter monitoring.
- Object Color Index B-V, used by the pipeline for calibration of the activity index $\log(R'_{HK})$;
- guess Radial Velocity (km/s), used by the pipeline in the calculation of the RV and activity index $\log(R'_{HK})$ determination;
- Object Spectral Type (e.g. G2), used by the pipeline to select a template for color correction and the correlation mask for the calculation of RV; Allowed values are: 'F9', 'G2', 'G8', 'G9', 'K2', 'K6', 'M0', 'M2', 'M3', 'M4' or 'M5'.
- Object Redshift from emission lines, used by the pipeline to shift the spectra of distant objects to our reference frame.
- FWHM measurement, to toggle Image Quality measurement during acquisition ON/OFF; default is OFF.

The instrument-specific comment field of the OB should include the expected S/N at a wavelength of 550 nm as reported by the ETC.

Science template:

- Binning/Readout Mode, used in the readout of the detector.
- Source on Fiber B, to define simultaneous reference. The available options are SKY and FPCS. The Fabry-Pérot calibration source (FPCS) is used for relatively bright targets and RV studies that require simultaneous drift measurement. The SKY option is used for faint targets for which a sky subtraction is required and/or for which a contamination from the FPCS light needs to be avoided;
- Number of exposures / Integration time of exposure.

7.2.2 Finding Charts

The unobstructed Field-of-View for the target acquisition has a radius of 17″. Finding charts should display a field of 30x30″ in the V band.

The distance between Fibre A and Fibre B is 7″. Due to the field rotation while observing, the Fibre B will rotate around the position of Fibre A. The finding chart generation in P2 shows an annulus for Fibre's B possible positions on the field of view, which can be checked for potential contamination of a nearby source.

7.2.3 Limiting magnitude for acquisition

Acquisition has succeeded with sources of V magnitudes as faint as 20 to 21 in dark sky. Acquisition of targets with magnitudes fainter than 18 require approval through a waiver.

7.2.4 Using Blind Offsets

Targets fainter that the limiting magnitude (V=18 and V=20 for the HR and MR mode, respectively) **must** be acquired using a blind offset. The convention is to provide the blind offsets in the acquisition template to move the telescope from the target to the acquisition star. **The coordinates of the science target must be entered in the OB target description**. In the acquisition template of the OB, the offsets of the acquisition star must be entered in arcseconds (target coordinates + offsets = acquisition star coordinates). If a blind offset is used, the magnitude of the acquisition star must also be provided.

Field stabilization can only be done on the science target. Targets using blind offsets are, by construction, often too faint for Field Stabilization with ESPRESSO. Since the Field Stabilization compensates for the drift of the Coudé Train Optics, not using Field Stabilization leads to a pointing error that translates into flux losses. To minimize this, observations using blind offset should select time windows to avoid meridian crossing and fast field rotation. For integration times of 10 min the pointing error is negligible. However, on integrations of 20 min one loses 5-10% of the predicted flux and on integrations of 30 minutes one loses 10-30%. Investigations on the matter continue, and these values should be taken as preliminary.

7.2.5 OB constraints

In Service Mode (SM) OBs are provided with observational constraints. We review three aspects of particular interest to ESPRESSO.

Operational airmass limit

ESO's VLT can observe down to an elevation of 20 degrees, i.e., an airmass of 2.9. However, the airmass limit for optimized ESPRESSO operations is imposed by the Atmospheric Dispersion Correctors (ADC's) limit. The ADC's were designed for a maximum airmass of 2.2. If a user chooses to observe a star at a higher airmass, the ADC will be configured for the maximum value of 2.2; the remaining uncorrected dispersion will be present in the observed spectrum. A loss of flux may result from centering errors, the SED may be affected, and with it the RV.

For reference, at an airmass of 2.2 the amplitude of the dispersion correction residuals on the position of the star on the sky is of approximately of 0.030 arcsec. If the airmass is larger

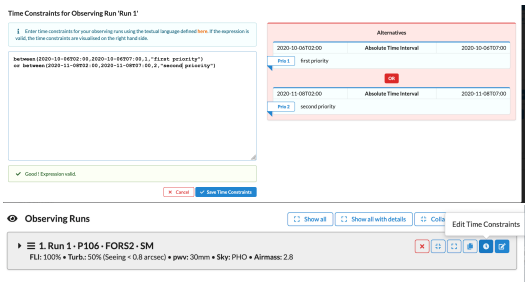

Figure 27: Example of a Time Critical OB absolute interval definition through syntax (*top*) and location of the online help for the absolute interval definition syntax (*bottom*).

than 2.2, for every additional 0.1 in airmass the dispersion grows by approximately 0.150″.

Fractional lunar illumination (FLI) and angular lunar separation

Observations with ESPRESSO are possible for the entire FLI range, although it is highly recommended to avoid to observing close to the moon at higher FLI. With Fiber B on sky, one is able to monitor and correct the contribution of lunar light in the science fiber. Although there is no hard limit to how close to the moon one can observe, it is again highly recommended to avoid observing very close to the moon, since otherwise difficulties are introduced to the guiding system. By default the angular separation is set to 30° and we recommend that the users do not go below this limit.

Lunar radial velocity

The radial velocity of the moon may be an important constraint for some ESPRESSO observations, but it is not directly a part of the ESO constraint set. Such a constraint needs to be translated into absolute time constraints to be provided in the time critical section of the Phase 1 proposal, and into absolute time constraints in the OBs at Phase 2.

Defining Local Sidereal Time and Absolute time interval constraints

It is important to keep in mind that while the Local Sidereal Time (LST) constraints are defined for the entire OB, the absolute time intervals are defined for the start of the OB. This distinction is particularly important for observations aiming at covering transient events, like planetary transits. We recommend users to request enough time to cover the target for their scientific purpose PLUS a reasonable interval in which the OB can be started (∼30min). This extra time requested provides an additional baseline for observations and makes the execution of OBs easier.

If stringent absolute time intervals are required for the successful execution of the program (e.g. planetary transits lasting more than 1hr with less than 10 opportunities in the period), users should include them in the Phase 1 proposal using the run definition syntax (and not only in the free text in the Box 'Time Justification'). Only in this way can the scheduler take the constraints into account. For the an example syntax and where to get online help on it through P1 interface take a look at Fig 27.

The effect of Precipitable Water Vapour

Precipitable Water Vapour (PWV) is the amount of water in gaseous form along a given

column in the Earth atmosphere. Measured as a depth, it corresponds to the value one would measure if all the water in that column would precipitate as rain. By knowing the PWV value during an observation and other parameters such as site altitude, temperature vertical profile, and humidity vertical profile, one can estimate the transmission spectra of water at any given wavelength. This predicting ability has been used extensively to measure and correct near-IR spectra, where water absorption band lines are deep and numerous.

In the ESPRESSO wavelength range we can find three main telluric absorption species: O_2, OH and H_2O. Of these, water vapour is the species that affects the widest wavelength range. Its effects are not as pronounced as in the near-IR, but may have an impact on specific science cases. For reference, the median Paranal PWV value is 2.5 mm, ranging between 0.5 mm and 20 mm in extremely favourable (dry) and unfavourable conditions (humid), respectively. For wavelengths shorter than 700 nm, water absorption amplitude is at the percent level if the PWV value is of 2.5 mm or lower, while for higher PWV values the depth of the water lines can reach up to 10%. On the other hand, the 700-800 nm wavelength range is strongly affected by water absorption, with numerous deep lines that can have an impact on the observations even in low PWV conditions. The user is referred to Querel, Naylor & Kerber (2011, PASP, 123, 222) and Kerber et al. (2014, MNRAS, 439, 247) for more information. If aiming at a high-spectral fidelity, the user should estimate the impact of the water vapour on the lines or wavelength ranges of interest. To this end, ESO provides two public tools; the SkyCalc Sky Model Calculator:

`https://www.eso.org/observing/etc/bin/gen/form?INS.MODE=swspectr+INS.NAME=SKYCALC`

which allow to measure the impact of the PWV and other observing conditions based on the Cerro Paranal Sky Model (Noll et al., 2012, A&A, 543, A92; Jones et al., 2013, A&A, 560, A91), and Molecfit (Smette et al., 2015, A&A, 576, A77):

`https://www.eso.org/sci/software/pipelines/skytools/molecfit`

which corrects astronomical observations for telluric absorption features, based on fitting synthetic transmission spectra calculated through a radiative transfer code. Users interested in spectral regions affected by deep telluric lines in the 700-800 nm domain or aiming at high spectral fidelity may request a specific constraint on the PWV when preparing their OBs during Phase 2. Since P105, the ESPRESSO ETC also includes PWV as an input.

7.2.6 Time series

When preparing time series of observations, one can define OBs inside a *Time-Link* container and provide absolute or relative time windows on when each OB can be executed.

The simplest way of defining constraints is through an absolute time constraint for the first OB of the series and relative time constraints for the following ones. However, users who want to minimize the number of OBs that are not executed within time constraints (called *Failed OBs*) should make sure that the respective constraints do not collide with telescope unavailability (e.g. VLTI 4UT runs). We have two cases:

- if we can accept having gaps (*Failed OBs*) in our time series, we can submit an absolute constraint for the first OB (considering only the target observability), and for the other OBs apply time constraints relative to the first OB. OBs that cannot be observed will be replaced at the end of the series after an iteration with the USD department.

- if we want to maximize the number of OBs executed, we need to adjust the starting point and the interval between OBs: can we define an absolute time constraint for the starting OB so that no OB on the time series falls on nights when no UTs are available? Can we use different intervals between OBs to avoid nights on which no telescope is available?

The list of the nights available for SM can be found on the telescope schedule page.

Note that there will always be a fraction of OBs lost to weather or technical issues, or simply due to higher-ranked programs being observed on the same time slot. When using *Time-Link* containers, please specify in the corresponding *README* file if it will be scientifically useful to recover any failed observations by adding replacement OBs at the series' end.

7.2.7 Common mistakes to avoid when preparing the observations

The most common mistakes to avoid are:

- **using FAST1x1 mode when trying to detect small-amplitude signals**: FAST1x1 should be selected only when the read-out error is negligible when compared to the photon noise and the signals to detect. On top of the additional white noise when compared to SLOW2x1, it contains additional correlated noise (see, e.g. Allart et al. 2020, Sedaghati et al. 2021) and should be avoided when attempting to detect small-amplitude signals.
- **scaling RV precision from previous observations instead of using the ETC**: ETC RV predictions, while imperfect (not containing models of all spectral types, or the impact of *v.sini*), provide a good estimate across spectral types and were updated to reflect the transmission changes after the intervention of July 2019. Scaling should only be made from observations taken after the intervention and on a star with the same spectral type and *v.sini* as the target to observe.
- **in time links with observations a few days apart, requesting an observational frequency much higher than the turbulence category probability**: the user should be very conservative when selecting meteorological conditions that are met rarely, as this will lead to a high rate of failed OBs. While at the observatory we have some latitude to trigger the OBs when the conditions are met, this is in natural conflict with the relative time constraints.

7.3 A summary of observations

Observing with ESPRESSO is very simple, and we describe briefly the procedure. Note though that the observations are not executed by the visiting astronomer, and this information is provided for completeness and reference for demanding programs.

7.3.1 The Acquisition

The exposure starts with the acquisition template, that configures several instrument parameters and triggers the acquisition on the target. The Telescope and Instrument Operator (TIO) will select the guide star if specified in the acquisition template; otherwise a guide star from

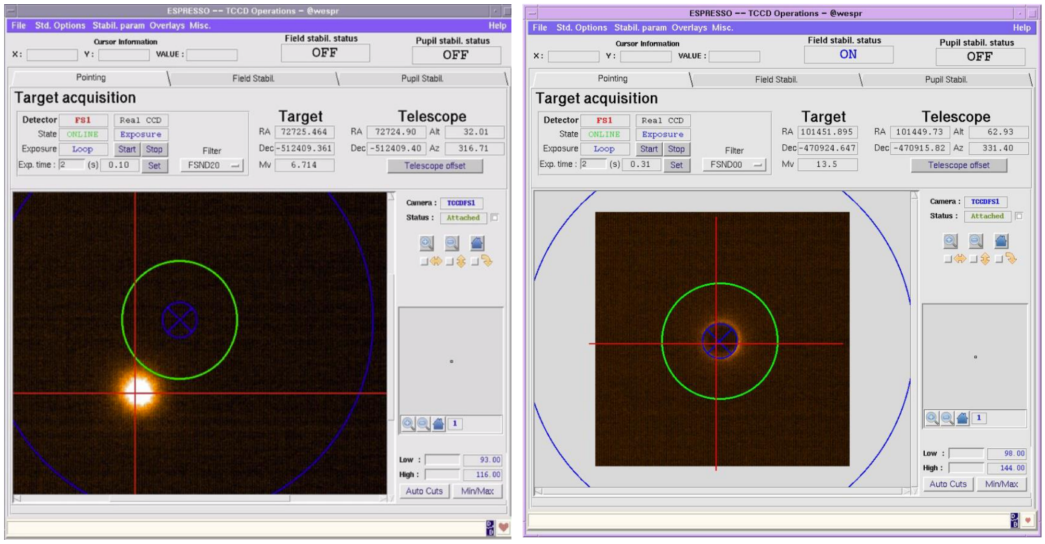

Figure 28: First step of the acquisition: selecting the scientific target on the field (*left*) and centering the star on the fibre (*right*).

a catalog will be selected. This implies juggling with several criteria: selecting a star bright enough for telescope guiding on short integration times, as close as possible to the scientific target, and with an available tracking time longer than the total time on target.

After the telescope guide star is selected and the telescope starts guiding, the telescope's central Field of view (FOV) is imaged on ESPRESSO's FE Field Technical CCD (TCCD). The TIO or Night Astronomer (NA) select the scientific target (using a FC if necessary), and the instrument's software sends an offset to the telescope to put the scientific target on the center of the instrument's FoV, over the fiber (Fig. 28).

If FWHM measurement is enabled, the Tip-Tilt mirror in the FE is used to move the star from behind the fibre (while keeping the telescope pointing to the star) and in this position measure the FWHM of the star on the TCCD. This provides an estimation of the Image Quality (IQ) as seen at the entrance of the spectrograph and can be used to estimate slit losses accurately. The measurement takes approximately 40s.

Afterwards, a feedback loop is activated using the TT mirror. The barycenter of the star is measured on the TCCD and compared with the position of the fiber; if these differ, a correction factor is applied on the TT to put the star on the fiber position. For efficiency, the TCCD is windowed over an area approximately 5″ by 5″ across. This procedure is looped to ensure a real-time correction of the position on the star, positioning it behind the fiber and minimizing centering errors. At this point in the acquisition the TIO/NA can enable or disable this positive feedback mechanism, called *Field Stabilization*, before passing into the Integration phase.

If a blind offset was provided, it is applied at this stage.

7.3.2 The Exposure Meter

ESPRESSO spectrograph is equipped with an Exposure Meter (EM) to measure the flux entering the spectrograph as a function of time.

It operates by focusing the light that is not injected into the spectrograph's fiber on a simple diffraction grating. This chromatic measurement permits a rough flux measurement over

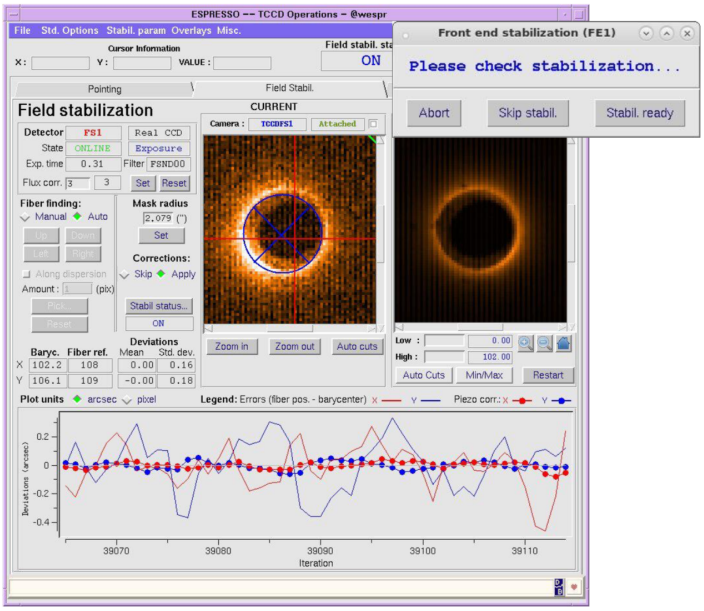

Figure 29: Second step of the acquisition: activating the Field Stabilization in the scientific target.

different spectral channels that can be used to identify possible chromatic effects. The use of several channels also provides a redundant, and thus more reliable, evaluation of the mean exposure time. In Fig. 30, one can see the EM graphical user interface (GUI). The efficiency and flux-weighted mean exposure time are stored in the FITS header of the scientific images.

The EM is automatically activated during an integration on the scientific detector.

The EM measurements are necessary to calculate the flux-weighted mean exposure time. This value should be defined accurately to calculate and remove the relative Earth motion component from the RV measurement.

7.3.3 The Integration

The integration step is done by one or several integration templates. These specify the source on fiber B, the readout mode of the detector, the number of exposures and its duration.

7.3.4 Quality Control – QC0

The data acquired at the telescope are reduced on real-time in order to provide a first quality control of observations. This *Quality Control 0* checks for basic parameters such as S/N and the fulfillment of observational constraints. Since reduction at the telescope does not use the most up-to-date calibration products, the data products cannot be considered final or science-graded.

7.4 Preparing observations and Observing with 4UT

Preparations of OBs and observations with 4UT are very similar to those on 1UT; they use templates *MULTIMR* but are otherwise identical. When using 4UT, it is recommended that the users select a *Guide Star* using the p2/ObsPrep tool to ensure that the same guide star is

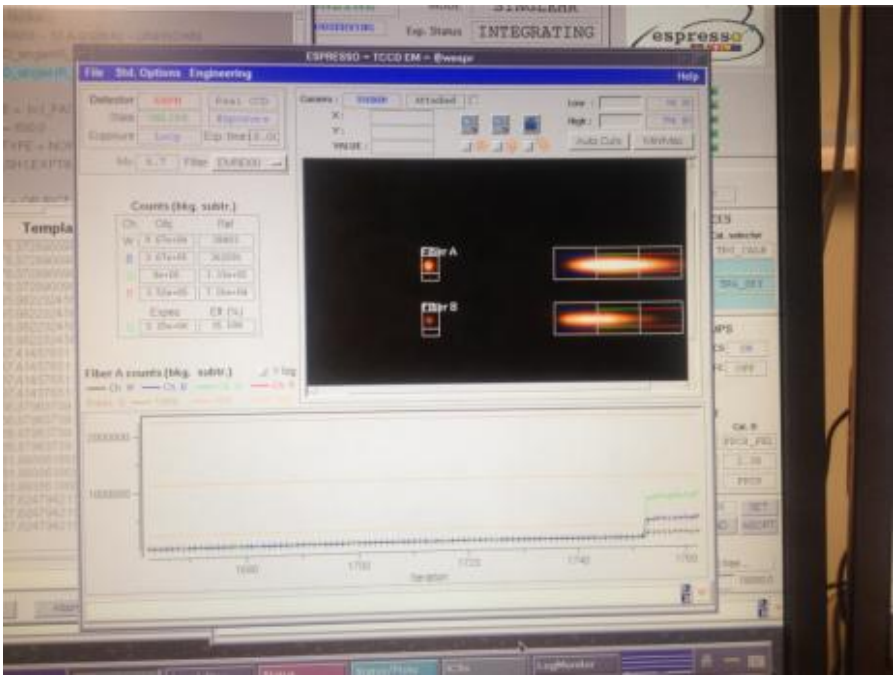

Figure 30: GUI of the exposure meter during observations.

selected on the 4 UTs. This reduces the number of Guide Star changes during the integration, reducing the pointing and tracking errors.

Acquisition is performed on each of the UTs simultaneously, with telescope preset being performed in parallel and Field Stabilization being performed sequentially. As such, the acquisition overheads on 4UT / MULTI MR are slightly longer.

8 Calibration Plan

Standard calibrations in the three singleHR modes (1x1, 2x1 and 4x2) are executed every day. Besides providing a full set of calibrations, these daily exposures are used for the instrument's health check. Standard calibrations for singleUHR and multiMR configurations will be executed within 24 hours of any science observations using these modes.

Science data in any configuration can be fully calibrated with a set of 11 different exposure types, *as provided by the standard calibrations.*

When processed by the ESPRESSO pipeline, each type of calibration frames generates several high-level Quality Control (QC1) parameters for instrument monitoring purposes.

The extreme precision and accuracy aimed for ESPRESSO can only be guaranteed if a full set of standard calibrations is obtained and passes quality control within 24 hours of any science observation. This 24-hour requirement is set by considering the timescales of instrument instabilities, partly based on the HARPS experience. An example is the RV drift of the spectrograph, which is expected to be below $\sim 1\,\mathrm{m/s}$.

This calibration plan should be sufficient for the majority of use cases. Observers interested in highest S/N may request additional flat-field frames. The calibration plan provides flat-field frames with a S/N of about 1000.

In case that the highest possible accuracy, such as flat-fielding accuracy, is required, the use of **attached calibrations** at nighttime is possible. However, the execution time will be charged to the corresponding program.

All possible types of **nighttime calibrations** (spectrophotometric standards, radial-velocity standards, telluric standards, etc.) must be specifically requested by the users. OBs for these calibrations must be supplied by the user. The time needed to execute these OBs will be charged to the user. *Note 1*: the `ESPRESSSO_<mode>_obs_std` templates are only to be used for flux standards. Radial velocity or telluric star observations have to be defined with the normal science templates `ESPRESSO_<mode>_obs_exp`. *Note 2*: **the use of either the ThAr or LFC is not permitted for nighttime calibration**.

Long-term calibrations are executed less frequently, typically once per month or less; these are executed for all supported instrument configurations. Table 6 describes the ESPRESSO standard calibration plan.

The pipeline can associate and use fibre-to-fibre relative efficiency and Spectro-Photometric calibrations taken on any UT. For an accurate sky subtraction and absolute flux calibration, please use relative efficiencies and spectrophotometric calibrations taken on the same UT as your science. The differences from one UT to the other are currently under investigation.

The execution of standard calibration sequences and long-term calibrations from the ESPRESSO calibration plan is under the responsibility of Paranal Science Operations. OBs for any additional day or night-time calibrations beyond the ESPRESSO calibration plan should be prepared by the user. Telescope time for any additional on-sky calibrations should be included in the total time allocation of the program.

The execution of calibrations for the Observatory can take up to 30 min of night time on any night on any UT (including VM nights). VM users should be aware that their time allocation can be reduced by this value.

Calibration type	Frequency	# of frames	Comments
Detector bias	Daily for singleHR within 24 hours of science for singleUHR and multiMR	10	Bias frames to measure over-scan, bias level and RON
Order definition	Daily for singleHR within 24 hours of science for singleUHR and multiMR	2 (1 p/fibre)	Continuum-source spectra on science and reference fibres to trace order/slice positions
Flat-field, blaze and order profile	Daily for singleHR modes within 24 hours of science for singleUHR and multiMR	20 (10 p/fibre)	Continuum-source spectra on science and reference fibres to measure spectral flat-field, blaze function and order profile in cross-dispersion direction.
Wavelength calibration	Daily for singleHR modes; within 24 hours of science for singleUHR and multiMR (except for the LFC)	1 p/setup	Lamp setups for the two fibres: FP_FP, THAR_FP, FP_THAR, LFC_FP, FP_LFC
Contamination by simultaneous reference	Daily for singleHR modes within 24 hours of science for singleUHR and multiMR	1	Depends on source used for drift FP is used as baseline since P102: Fibre A: CONTAM (no light) Fibre B: FP
Detector dark current	Monthly for all modes	5 (x 3600s)	Dark frames to measure the average dark current and create the hot-pixel mask.
Detector flat-field and gain	Every 2 months for all modes	15	Detector LED flat-field frames to measure the gain and create a bad-pixel map.
Fibre-to-fibre relative efficiency	Quarterly for singleHR and singleUHR multiMR only when in 4UT VM	1	Blue-sky observations with both fibres to measure the relative efficiency: Fibre A: SKY Fibre B: SKY
Spectro- photometric calibration	Every 120 days for singleHR and singleUHR; multiMR only when in 4UT VM	1	Observation of a spectro-photometric standard star to measure the absolute efficiency on any UT: Fibre A: sp.-phot. standard star Fibre B: SKY
RV standard	Every 7 days for singleHR 1x1 and 2x1	2 or 10	Observation of RV standard to monitor long-term instrumental stability Fibre A: RV standard star Fibre B: FP

Table 6: ESPRESSO Calibration Plan.

9 Software for an End-to-End Operation

The ESPRESSO instrument was designed along with a complete software suite. The final objective is to provide the observer with a complete science-graded dataset, increasing the efficiency and scientific output of the instrument. For this purpose, a software-cycle integrated view was adopted, from the preparation of the observations to the data reduction and analysis. The ESPRESSO Data Flow System (DFS) includes the following main components:

- ESO's *p2* tool for Phase-2 preparation.
- Specific instrument control and observation templates: ESPRESSO is compliant with the usual VLT control software environment and concepts. Compared to other VLT instruments, ESPRESSO's operational complexity arises from the ability to use any combination of UTs. At the instrument control level, PLCs (Programmable Logical Controllers), as well as off-the-shelf TCCDs, place ESPRESSO at the forefront of current instrument control systems.
- The DRS (Data Reduction Software) and DAS (Data Analysis Software): a brief description of these is given below. The interested reader is referred to the corresponding reference documents for more detailed information.

For more information on the pipeline refer to

Pepe et al. (2020) "ESPRESSO@VLT – On-sky performance and first results"

The ESPRESSO pipeline installed at Paranal is meant for a quick assessment of data quality. It does not make use of the latest calibration projects or is optimized in any way to provide science-graded data. In order to obtain high-quality reduced data, the user should install the pipeline, and make use of the properly associated calibrations.

9.1 Data Reduction Software (DRS)

ESPRESSO is provided with a data-reduction software (DRS) pipeline to deliver high-quality science-grade reduced spectra. The final products of the DRS are extracted wavelength-calibrated spectra, along with the RV. If the fiber B is pointed to the sky, an additional data product provides sky-subtracted data; if fiber B is used for simultaneous RV monitoring, the drift is calculated and applied to the calculated RV. The extracted spectra can also be flux calibrated if associated to spectro-photometric standards.

9.2 Data Analysis Software (DAS)

The ESPRESSO DAS is the first dedicated data analysis system for an ESO instrument and is meant to work in close interaction with the ESPRESSO DRS. While the DRS is automatically triggered by the generation of new observational raw data files, the DAS allows users to manipulate the reduced data in an interactive way.

The DAS comprises a total of 13 recipes tailored to the ESPRESSO main science cases. It is split into four branches: one for the analysis of quasar spectra, and three for the analysis of stellar spectra. Each branch of the DAS is managed by a Reflex workflow. The recipes take

care of complex analysis operations, e.g., for stellar spectra: the estimation of stellar activity indices and stellar parameters (effective temperature, [Fe/H] ratio), the measurement of the equivalent widths of absorption lines, the fitting of the stellar continuum, and the re-calculation of radial velocities based on user needs; for quasar spectra: the optimal co-addition of multiple exposures, the detection of absorption lines, the determination of the QSO continuum level, and the identification and fitting of absorption-line systems.

9.3 Pipeline results across architectures

Different third-party software and system compilers can introduce small systematic differences on the calculated RV and associated uncertainties. Analysis of the same dataset on a Fedora installation on a laptop versus a HighSierra on a Macintosh showed an offset of 4 cm/s in the RV. Being an offset and not a source of numerical error, this difference has no impact on the instrument precision; additionally, this offset is smaller than the ultimate RV precision of ESPRESSO and much smaller than the its RV accuracy. However, if the results of several datasets have to be compared, it is highly recommended to reduce those datasets with the same pipeline version and the same hardware.

For the installation and usage of the DRS and DAS, the reader is referred to the ESO pipeline pages

http://eso.org/sci/software/pipelines/

and to the latest ESPRESSO pipeline user manual and tutorials.

Appendix A ESPRESSO Spectral Format

Table 7 and Table 8 describe the spectral format recorded by each of the detectors, as provided by the ESPRESSO ETC. For each order number, from left to right, the wavelength of the central column, the free spectral range (FSR) size, the minimum and maximum wavelengths, the order starting and ending wavelengths and size, and the template spectra (TS) range, are given.

When comparing the ETC output with DRS products, be aware that the order numbering is different:

- *interference orders vs numbered orders on the detector*: while ETC numbers the orders using the physical interference orders m, the DRS products have their orders numbered from 1, starting from the bluest one;
- *single orders versus double orders in* singleHR *and* singleUHR: while the ETC considers interference orders, the DRS products contain the two individual orders imaged on the detector for each of the interference order (see Sect. 3.3 for details). As such, the S/N reported by the ETC corresponds to the quadratic sum of the two orders in the DRS products.

ETC/Int. Order	HR/UHR Orders	MR Order	Central wav.[nm]	FSR range[nm]	FSR min[nm]	FSR max[nm]	start wav[nm]	end wav[nm]	TS range[nm]
117	89,90	45	522.97	4.47	520.74	525.21	519.13	527.03	7.89
118	87,88	44	518.54	4.39	516.35	520.74	514.72	522.57	7.84
119	85,86	43	514.18	4.32	512.03	516.35	510.39	518.18	7.79
120	83,84	42	509.89	4.25	507.78	512.03	506.13	513.87	7.74
121	81,82	41	505.68	4.18	503.60	507.78	501.94	509.63	7.69
122	79,80	40	501.53	4.11	499.49	503.60	497.82	505.45	7.64
123	77,78	39	497.46	4.04	495.44	499.49	493.76	501.35	7.58
124	75,76	38	493.44	3.98	491.46	495.44	489.78	497.31	7.53
125	73,74	37	489.50	3.92	487.55	491.46	485.85	493.33	7.48
126	71,72	36	485.61	3.85	483.69	487.55	481.99	489.42	7.43
127	69,70	35	481.79	3.79	479.90	483.69	478.19	485.57	7.38
128	67,68	34	478.02	3.73	476.16	479.90	474.45	481.78	7.33
129	65,66	33	474.32	3.68	472.49	476.16	470.77	478.05	7.28
130	63,64	32	470.67	3.62	468.87	472.49	467.15	474.38	7.23
131	61,62	31	467.08	3.57	465.30	468.87	463.57	470.76	7.18
132	59,60	30	463.54	3.51	461.79	465.30	460.06	467.19	7.13
133	57,58	29	460.05	3.46	458.33	461.79	456.60	463.68	7.08
134	55,56	28	456.62	3.41	454.92	458.33	453.19	460.22	7.04
135	53,54	27	453.24	3.36	451.57	454.92	449.83	456.82	6.99
136	51,52	26	449.91	3.31	448.26	451.57	446.52	453.46	6.94
137	49,50	25	446.62	3.26	445.00	448.26	443.26	450.15	6.90
138	47,48	24	443.39	3.21	441.78	445.00	440.04	446.89	6.85
139	45,46	23	440.20	3.17	438.62	441.78	436.87	443.68	6.81
140	43,44	22	437.05	3.12	435.50	438.62	433.75	440.51	6.76
141	41,42	21	433.95	3.08	432.42	435.50	430.67	437.39	6.72
142	39,40	20	430.90	3.03	429.38	432.42	427.64	434.31	6.67
143	37,38	19	427.88	2.99	426.39	429.38	424.64	431.27	6.63
144	35,36	18	424.91	2.95	423.44	426.39	421.69	428.28	6.59
145	33,34	17	421.98	2.91	420.53	423.44	418.78	425.33	6.55
146	31,32	16	419.09	2.87	417.66	420.53	415.91	422.42	6.50
147	29,30	15	416.24	2.83	414.83	417.66	413.08	419.54	6.46
148	27,28	14	413.43	2.79	412.03	414.83	410.29	416.71	6.42
149	25,26	13	410.65	2.76	409.28	412.03	407.53	413.91	6.38
150	23,24	12	407.91	2.72	406.56	409.28	404.82	411.15	6.34
151	21,22	11	405.21	2.68	403.88	406.56	402.13	408.43	6.30
152	19,20	10	402.55	2.65	401.23	403.88	399.48	405.75	6.26
153	17,18	9	399.92	2.61	398.61	401.23	396.87	403.10	6.22
154	15,16	8	397.32	2.58	396.03	398.61	394.30	400.48	6.18
155	13,14	7	394.76	2.55	393.49	396.03	391.75	397.90	6.15
156	11,12	6	392.23	2.51	390.97	393.49	389.24	395.35	6.11
157	9,10	5	389.73	2.48	388.49	390.97	386.76	392.83	6.07
158	7,8	4	387.26	2.45	386.04	388.49	384.31	390.34	6.03
159	5,6	3	384.83	2.42	383.62	386.04	381.89	387.89	6.00
160	3,4	2	382.42	2.39	381.23	383.62	379.50	385.47	5.96
161	1,2	1	380.04	2.36	378.87	381.23	377.15	383.07	5.93

Table 7: Spectral format of ESPRESSO's blue CCD.

ETC/Int. Order	HR/UHR Orders	MR Order	Central wav.[nm]	FSR range[nm]	FSR min[nm]	FSR max[nm]	start wav[nm]	end wav[nm]	TS range[nm]
78	169,170	85	784.45	10.06	779.45	789.51	778.98	790.64	11.66
79	167,168	84	774.52	9.80	769.65	779.45	769.11	780.65	11.54
80	165,166	83	764.84	9.56	760.09	769.65	759.48	770.89	11.41
81	163,164	82	755.40	9.33	750.76	760.09	750.10	761.38	11.28
82	161,162	81	746.19	9.10	741.66	750.76	740.95	752.10	11.16
83	159,160	80	737.19	8.88	732.78	741.66	732.01	743.04	11.03
84	157,158	79	728.42	8.67	724.11	732.78	723.29	734.20	10.91
85	155,156	78	719.85	8.47	715.64	724.11	714.78	725.57	10.79
86	153,154	77	711.48	8.27	707.37	715.64	706.46	717.13	10.67
87	151,152	76	703.30	8.08	699.28	707.37	698.34	708.89	10.56
88	149,150	75	695.31	7.90	691.38	699.28	690.40	700.84	10.45
89	147,148	74	687.50	7.72	683.66	691.38	682.63	692.97	10.34
90	145,146	73	679.86	7.55	676.10	683.66	675.04	685.27	10.23
91	143,144	72	672.39	7.39	668.71	676.10	667.62	677.74	10.12
92	141,142	71	665.08	7.23	661.48	668.71	660.36	670.38	10.02
93	139,140	70	657.93	7.07	654.41	661.48	653.26	663.18	9.92
94	137,138	69	650.93	6.92	647.48	654.41	646.31	656.12	9.82
95	135,136	68	644.08	6.78	640.70	647.48	639.50	649.22	9.71
96	133,134	67	637.37	6.64	634.06	640.70	632.84	642.46	9.62
97	131,132	66	630.80	6.50	627.56	634.06	626.31	635.83	9.52
98	129,130	65	624.36	6.37	621.19	627.56	619.92	629.35	9.43
99	127,128	64	618.05	6.24	614.95	621.19	613.65	622.99	9.34
100	125,126	63	611.87	6.12	608.83	614.95	607.52	616.76	9.25
101	123,124	62	605.81	6.00	602.83	608.83	601.50	610.66	9.16
102	121,122	61	599.87	5.88	596.95	602.83	595.60	604.67	9.07
103	119,120	60	594.05	5.77	591.18	596.95	589.82	598.80	8.99
104	117,118	59	588.34	5.66	585.52	591.18	584.14	593.05	8.90
105	115,116	58	582.74	5.55	579.97	585.52	578.58	587.40	8.82
106	113,114	57	577.24	5.45	574.53	579.97	573.12	581.86	8.74
107	111,112	56	571.84	5.34	569.18	574.53	567.76	576.42	8.66
108	109,110	55	566.55	5.25	563.94	569.18	562.50	571.08	8.58
109	107,108	54	561.35	5.15	558.79	563.94	557.34	565.85	8.51
110	105,106	53	556.25	5.06	553.73	558.79	552.27	560.71	8.43
111	103,104	52	551.24	4.97	548.76	553.73	547.30	555.65	8.36
112	101,102	51	546.31	4.88	543.89	548.76	542.41	550.69	8.29
113	99,100	50	541.48	4.79	539.09	543.89	537.61	545.82	8.22
114	97,98	49	536.73	4.71	534.39	539.09	532.89	541.03	8.15
115	95,96	48	532.06	4.63	529.76	534.39	528.25	536.33	8.08
116	93,94	47	527.48	4.55	525.21	529.76	523.70	531.71	8.01
117	91,92	46	522.97	4.47	520.74	525.21	519.22	527.16	7.94

Table 8: Spectral format of ESPRESSO's red CCD.